Comparative toxicity of three differently shaped carbon nanomaterials on Daphnia magna: does a shape effect exist?

Journal:	*Nanotoxicology*
Manuscript ID	Draft
Manuscript Type:	Original Article
Date Submitted by the Author:	n/a
Complete List of Authors:	BACCHETTA, RENATO; Università degli Studi di Milano, Dipartimento di Scienze e Politiche Ambientali Santo, Nadia; Università degli Studi di Milano, Dipartimento di Bioscienze Valenti, Irene; Università degli Studi di Milano, Dipartimento di Scienze e Politiche Ambientali Maggioni, Daniela; Universita degli Studi di Milano, Dipartimento di Chimica Longhi, Mariangela; Università degli Studi di Milano, Dipartimento di Chimica Tremolada, Paolo; Università degli Studi di Milano, Dipartimento di Scienze e Politiche Ambientali
Keywords:	Nanotoxicology, Carbon nanoparticles, Carbon nanocubes, Carbon nanotubes, Microscopy
Abstract:	The acute toxicity of three differently shaped carbon nanomaterials, CNMs, was studied on Daphnia magna, comparing the induced effects and looking for the toxic mechanisms. We used carbon nano-powder, CNP, with almost spherical primary particle morphology, multi-walled carbon nanotubes, CNTs, tubes of multi-graphitic sheets, and cubic-shaped carbon nanoparticles, CNCs, for which no ecotoxicological data are available so far. Daphnids have been exposed to six suspensions (1, 2, 5, 10, 20 and 50 mg L-1) of each CNM, and then microscopically analyzed. Ultrastructural analyses evidenced nanoparticle internalization only in CNP and CNT exposed groups. Despite the different CNM morphologies, very similar effects have been observed in tissues exposed to the selected

	nanoparticles: empty spaces between cells, cell detachment from the basal lamina, many lamellar bodies and autophagy vacuoles. CNCs caused additional effects, such as partial or complete dissolution of the brush border and thinning of the digestive epithelium. From our observations and according to the literature, it can be concluded that shape is an important factor for determining nanoparticle uptake and for general toxicity, being the cubic shape not allowed to be internalized into cells, and more effective than others in determining physical damages. On the contrary, looking at the effects at cellular level and considering the similar figures observed in different tissues, shape does not seem to be involved in determining the kind of the pathology, which may be due to the physical interactions of nanoparticles with the exposed tissues.

Comparative toxicity of three differently shaped carbon nanomaterials on *Daphnia magna*: does a shape effect exist?

Renato Bacchetta[1*], Nadia Santo[2], Irene Valenti[1], Daniela Maggioni[3], Mariangela Longhi[3] & Paolo Tremolada[1]

[1] *Dipartimento di Scienze e Politiche Ambientali, Università degli Studi di Milano, Via G. Celoria, 26, I-20133 Milan, Italy*

[2] *Dipartimento di Bioscienze, Università degli Studi di Milano, Via G. Celoria, 26, I-20133 Milan, Italy*

[3] *Dipartimento di Chimica, Università degli Studi di Milano, Via C. Golgi, 19, I-20133 Milan, Italy*

* Corrispondence:

Renato Bacchetta, Dipartimento di Scienze e Politiche Ambientali,

Università degli Studi di Milano, Via G. Celoria, 26, I-20133 Milan, Italy.

E-mail: renato.bacchetta@unimi.it - http://orcid.org/0000-0002-3328-0139

Tel +39 02 50314783 - Fax +39 02 50314781

Abstract

The acute toxicity of three differently shaped carbon nanomaterials, CNMs, was studied on *Daphnia magna*, comparing the induced effects and looking for the toxic mechanisms. We used carbon nano-powder, CNP, with almost spherical primary particle morphology, multi-walled carbon nanotubes, CNTs, tubes of multi-graphitic sheets, and cubic-shaped carbon nanoparticles, CNCs, for which no ecotoxicological data are available so far. Daphnids have been exposed to six suspensions (1, 2, 5, 10, 20 and 50 mg L^{-1}) of each CNM, and then microscopically analyzed. Ultrastructural analyses evidenced nanoparticle internalization only in CNP and CNT exposed groups. Despite the different CNM morphologies, very similar effects have been observed in tissues exposed to the selected nanoparticles: empty spaces between cells, cell detachment from the basal lamina, many lamellar bodies and autophagy vacuoles. CNCs caused additional effects, such as partial or complete dissolution of the brush border and thinning of the digestive epithelium. From our observations and according to the literature, it can be concluded that shape is an important factor for determining nanoparticle uptake and for general toxicity, being the cubic shape not allowed to be internalized into cells, and more effective than others in determining physical damages. On the contrary, looking at the effects at cellular level and considering the similar figures observed in different tissues, shape does not seem to be involved in determining the kind of the pathology, which may be due to the physical interactions of nanoparticles with the exposed tissues.

Keywords: Nanotoxicology; carbon nanoparticles; carbon nanocubes; carbon nanotubes; microscopy

Introduction

Carbon nanomaterials, CNMs, such as fullerenes, graphene nanoflakes, single-walled carbon nanotubes, SWCNTs, multi-wall carbon nanotubes, MWCNT, and carbon black, CB, are currently applied in a variety of fields, such as electronics, analytical chemistry, catalysis and nanomedicine,

and are recognized among the most promising nanoparticles in the near future (De Volder *et al.*, 2013, Sanchis *et al.*, 2016). Indeed, concerns have already been raised about the potential toxicity of these CNMs for both the environment and living organisms, man included (Mattsson *et al.*, 2016). Animal models, human cell lines and epidemiological researches have been used in toxicological studies (Magrez *et al.*, 2006, Pulskamp *et al.*, 2007, Yoshida *et al.*, 2009, Jackson *et al.*, 2013) and adverse effects on organisms and natural ecosystems have been observed in algae (Schwab *et al.*, 2011, Long *et al.*, 2012), mollusks (Canesi *et al.*, 2010), planktonic and benthonic crustaceans (Kennedy *et al.*, 2008), insects (Liu *et al.*, 2009), amphibians (Mouchet *et al.*, 2010, Bacchetta *et al.*, 2012), and fish (Oberdorster, 2004, Zhu *et al.*, 2006, Asharani *et al.*, 2008). Data from the literature suggested that oxidative stress, inflammation, and autophagy are the main toxic mechanisms in CNMs' cytotoxicity (Khanna *et al.*, 2015, Tsukahara *et al.*, 2015), even though results are not conclusive. Among the many physicochemical properties of nanoparticles, NPs, shape has been recognized to play a key role in the nano-bio interactions (Elder *et al.*, 2009), and many papers have investigated the toxicity of differently shaped nanomaterials. Most of these studies have been made using Au (Chithrani and Chan, 2007), Ni (Ispas *et al.*, 2009), Si (Huang *et al.*, 2011), Ag (George *et al.*, 2012) and Zn oxide NPs (Hua *et al.*, 2014), but the importance of the surface geometry in determining toxicity seems to be true also for CNMs. In fact, Gratton and co-workers using particles larger than 100 nm have reported that shape directly influences the entrance into cells, demonstrating that rods showed the highest uptake, followed by spheres, cylinders and cubes (Gratton *et al.*, 2008). Despite the experimental evidences, the debate on the role of shape in NP toxicity is still ongoing, also considering that the toxicity of different NP shapes is reported to be species-specific and composition-dependent too (Hua *et al.*, 2014).

In this work, we compare the toxic effects of three differently shaped carbon NPs on the planktonic crustacean *Daphnia magna*, focusing on the toxic mechanisms as deduced by electron microscopy analyses. *D. magna* is a well-established model for ecotoxicological studies (OECD, 2004, OECD, 2012), and it has already been used to study carbon NP toxicity (Lovern and Klaper, 2006, Kim *et*

al., 2009, Edgington *et al.*, 2014). We have studied two commercially available carbon-based NPs: carbon nano-powder, CNP, with almost spherical primary particle morphology and multi-walled carbon nanotubes, CNTs, tubes of multi-graphitic sheets. We additionally have considered a cubic-shaped carbon NP, CNC, recently synthetized by Marzorati and coworkers at the Department of Chemistry, University of Milan (Marzorati, 2015), and for which no ecotoxicological data are available so far. The acute toxicity of these three CNMs was studied focusing on the main possible uptake routes for *D. magna*. Therefore, we analyzed the epithelial tissues of gut and gills, considering that gut is a typical site for accumulation and internalization of NPs (Roberts *et al.*, 2007, Zhu *et al.*, 2009, Edgington *et al.*, 2010, Edgington *et al.*, 2014, Santo *et al.*, 2014, Bacchetta *et al.*, 2016, Bacchetta *et al.*, 2017), and that gills are considered uptake sites for fish and aquatic organisms as well (Handy *et al.*, 2008, Shaw and Handy, 2011, Hao *et al.*, 2013, Skjolding *et al.*, 2014). Despite their importance in gas exchanges and ion homeostasis (Kikuchi, 1983, Goldmann *et al.*, 1999, Paul *et al.*, 2004, Maas, 2009), it seems very likely that the thin epithelial barrier of *D. magna* gills might act as an entry route for NPs as well, but no study has considered this point so far. Our final goals were: *i*) studying the acute toxicity of the three chosen NPs comparatively; *ii*) checking if NP uptake happens in both the epithelial tissues of gut and gills; *iii*) looking at the possible morphological alterations induced by the three different CNMs; *iv*) investigating if there is NP translocation over the intestinal epithelium, and *v*) analyzing the possible role of the NP shape in determining toxicity.

Material and methods

CNM used and NP characterization

Three differently shaped carbon NPs were selected for this study: CNP, CNTs, and CNCs. CNP and CNTs were purchased from Sigma-Aldrich (Milano, Italy; CAS N. 7440-44-0 and 308068-56-6, and catalog N. 633100 and 698849, for CNP and CNT, respectively). According to the producer, CNP has a carbon content >99%, an advertised particle diameter <50 nm (TEM), and a specific

surface area >100 m^2 g^{-1} (BET); CNT has a carbon content >98%, diameter ranging from 6-13 nm and length from 2.5-20 µm. CNC were synthetized and characterized at the Department of Chemistry, University of Milan (Marzorati, 2015).

In order to obtain size frequency distribution diagrams, more than 1000 NPs from each differently shaped NM were measured in pictures taken by TEM at a magnification of 50000X, using the ImageJ software (Schneider *et al.*, 2012). CNP and CNT diameters (from 1290 and 1050 different samples, respectively), as well as one face from 1143 CNCs were measured. All NPs were first suspended in distilled water, stirred and then sonicated for 1 min. Aliquots of 3 µl were immediately pipetted and deposited onto Formvar®-coated 200 mesh copper grids, and excess of water was gently removed using filter paper. Once dried, grids were directly inserted into a Zeiss LEO 912ab TEM operating at 120 kV, and images were collected using a CCD-BM/1K system.

CNP, CNT and CNC were also analyzed for purity using a Zeiss LEO 1430 scanning electron microscope (SEM), coupled with a Centaurus detector for energy dispersive X-ray spectroscopy analysis (EDX). The same grids used for TEM analyses, were mounted onto standard SEM stubs and gold-coated. The elemental analysis was performed using the Oxford Instruments INCA ver. 4.04 software (Abingdon, UK). Operating conditions were: accelerating voltage 20 kV, probe current 360 pA, and working distance of 15.0 mm.

Hydrodynamic behavior of NPs and their extent of aggregation in the test medium were obtained by Dynamic Light Scattering (DLS) measurements. A Zetasizer Nano ZS instrument (Malvern, Worcestershire, UK) was used. For each considered NP, three suspensions in a commercial mineral water (San Benedetto®) at different concentrations (1, 10, and 50 mg L^{-1}) were prepared following the same procedure described below for the exposure experiments. Measurements were performed at 0, 0.5, 3, 6, and 24 h after sample preparation. Analyses were performed at 25 °C, using a laser beam incident light with a wavelength of 633 nm and at a detection angle of 173°. The refractive index and the viscosity of the solution were approximated to that of the pure solvent, water (used values: 1.33 and 0.8872, respectively), while the refractive index of solute was always set equal to

2.42 (RI of carbon black). The standard deviation of the hydrodynamic diameters was obtained from the mean width at half height of the intensity-based size distribution. Each measurement was repeated 4 times, and the reported values derive from the mean value of the significant measurements (intensity-based size distribution).

ζ-potential measurements were performed on the same Malvern Zetasizer Nano ZS instrument (endowed with the ζ-potential accessory) on the three carbon-NP suspensions in San Benedetto® mineral water at the concentrations of 1, 10 and 50 mg/L. Suspension preparation followed the same procedure described below for the exposure experiments.

Polycyclic Aromatic Hydrocarbons (PAHs) analysis

Extraction and analyses were performed as previously described (Bacchetta *et al.*, 2012). Briefly, About 10 mg of each carbon nanoparticle was extracted for 48h with toluene (Fluka, Steinheim, Germany) in soxhlet apparatus (FALC Instruments, Lurano, Italy). Samples were then concentrated, passed through an anhydrous sodium sulphate (Fluka, Steinheim, Germany) column and concentrated again to the final volume of 1.5 mL. An aliquot of 2 µL was injected into a GC chromatograph (TRACE GC, Thermo-Electron, Texas, USA) equipped with a programmed temperature vaporizer (PTV) injector, an AS 2000 autosampler (Thermo Electron) and a Rtx-5MS (Restek, Bellefonte, PA, USA) capillary column (30 m length, 0.25 mm I.D., 0.25 µm film thickness). The gas chromatograph was coupled with a PolarisQ Ion Trap mass spectrometer. PAHs were quantified by Selective Ion Monitoring (SIM) after Electron Ionisation (EI). Quantitative analyses were performed using Excalibur software (Thermo-Electron, Texas, USA) and by external calibration curves ranging from 1 to 100 pg μL^{-1}. PAH standards were purchased from Dr. Ehrenstorfer (Augsburg, Germany). Two injections were performed for standards and samples and mean quantification were considered. Quality assurance (QA) and quality control (QC) were performed by procedural blanks, replicates analyses and previous recovery tests using Standard Reference Materials (river sediment 1939a, NIST, Gaithersburg, MD). Each sample was injected

twice and replicate analyses of the same samples were performed. Mean instrumental precision was 14% (mean variation coefficient between injections) and mean analytical precision was 15% (mean variation coefficient between replicates). The recoveries for all compounds were always greater than 65% with respect to the reference value. The limits of detection (LODs) were estimated by the signal-to noise ratio (3:1) and ranged between 0.2 and 0.4 pg injected for each compound (0.015 and 0.03 μg g^{-1}, considering 10 mg extract and 2 μL injection). The limits of quantifications (LOQs) were calculated as 3 times the mean concentration in blanks and ranged between 0.36 and 34 μg g^{-1} depending on the compound. PAH concentrations in samples, over LOQs, were corrected by the mean concentrations in blanks.

Test species

The freshwater crustacean *Daphnia magna* Straus, originally obtained from the Istituto Superiore di Sanità (ISS, Roma, Italy) and maintained by the authors at the University of Milan, was used as test species. Specimens (30 ind L^{-1}) were cultured in a commercial mineral water (San Benedetto®, whose chemico-physical parameters were: conductivity 415 μS cm^{-1} at 20°C, pH 7.42, 301 mg L^{-1} HCO_3^-, 48.6 mg L^{-1} Ca^{2+}, 28.2 mg L^{-1} Mg^{2+}). They were fed a suspension of the unicellular green alga *Pseudokirchneriella subcapitata* (0- to 8-day-old daphnids: 8 x 10^6 cells ind^{-1} day^{-1} and from 8-day-old daphnids: 16 x 10^6 cells ind^{-1} day^{-1}) and the yeast *Saccharomyces cerevisiae* (15 x 10^6 cells mL^{-1}) three times a week during the culture medium renewal, when offspring was discarded and mothers transferred to the new medium. Cultured specimens were renewed every 5/6 weeks by replacing them with neonates. Daphnids from the fourth reproduction cycle were taken for culture renewal and for the exposure experiments. Culture and exposure solutions were maintained at 20.5 ± 0.5 °C under a 16 h light: 8 h dark photoperiod. According to Frey (Frey, 1982), the above conditions assure continuous amictic parthenogenetic reproduction in cultures. Algae were cultured in ISO 8692: 1989 medium within a 2L flask at 20 ± 2°C under continuous light and shaken by bubbling air. Algae were harvested during their exponential growth and left in the dark at 4°C for

sedimentation for 8 days. After supernatant elimination, cell density of the concentrated algal suspension was determined using a Burker counting chamber under a Zeiss light microscope.

Acute toxicity test

Exposure experiments run following the OECD 202 protocol (OECD, 2004). Three subsequent experiments were performed for the three selected NPs; for each NP, six exposure concentrations (1, 2, 5, 10, 20 and 50 mg L^{-1}) and two controls run together. Four replicates for each concentration and control were maintained for 48 h at 20.5 ± 0.5 °C under a 16 h light: 8 h dark photoperiod. Each replicate contains 5 *D. magna* neonates (less than 24 h old and almost of the third generation to limit variability) in 100 mL of mineral water, without feeding for 48 h. Oxygen concentration, pH, and mortality were checked in controls to ensure the validity of the tests. Oxygen and pH were measured before and after the experiment in each batch. Daphnids immobilization and viability were used as acute toxicity endpoints and were controlled in each batch at 24 and 48 h. According to the OECD 202 protocol (OECD, 2004) animals unable to swim within 15 s of gentle agitation of the test container were considered immobile, while those whose heartbeats have stopped were considered dead.

NP suspensions were prepared according to the protocol for NP dispersions suggested by (OECD, 2010). Briefly, 40 mg of each NP were weighted, initially dispersed in few drops of water medium, then in a volume of 20 mL. The obtained suspensions were sonicated for 30 s at 20 KHz ± 50 Hz, then diluted to 100 mL, sonicated again at the same conditions. These stock suspensions (400 mg L^{-1}) were diluted to obtain the final concentrations (from 50 to 1 mg L^{-1}). Stock suspensions and final dilutions were always sonicated, as above, after preparation and before use.

Light and electron microscopy

For each NP and used concentration, 10 specimens among those still alive at the end of the exposure test were randomly selected from the 4 replicates for histological and ultrastructural

analyses. They were fixed in a mixture of 2% paraformaldehyde 2% glutaraldehyde in 0.1 M sodium cacodylate buffered solution at pH 7.4. After washes with the same buffer, daphnids were postfixed in 1% OsO_4 for 1.5 h at 4° C, dehydrated in a graded ethanol series and finally in 100% propylene oxide. Infiltration was subsequently performed with propylene oxide resin (Araldite-Epon) at volumetric ratios of 2:1 for 1.5 h, 1:1 overnight, and 1:2 for 1.5 h. Daphnids were then embedded in 100% pure resin for 4 h, and polymerization was performed at 60°C for 48 h. Sectioning was performed using an Ultracut E microtome (Reichert, Austria): semithin sections of about 1 µm were collected onto microscope slides and stained with 1% toluidine blue to select the region of interest. The histological analysis was performed on semithin sections from 5 samples from each treatment group, control included. For the ultrastructural analysis, 10-15 ultrathin sections of 60-70 nm from the midgut and the gill region of each sample were collected on 600-mesh uncoated copper grids. Sections were not counterstained and observed with a Zeiss LEO 912ab Energy Filtering TEM operating at 120 kV. Digital images were acquired using a CCD-BM/1K system operating with the ESI vision software AnalySIS (Soft Imaging Systems, Muenster, Germany). For this analysis, 5 specimens from controls and from 1, 10 and 50 mg/L groups were considered, for a total of 20 daphnids for each NP.

In order to study in detail the morphology of gills and their relationships with the selected CNMs, at least 10 daphnids from controls and from 1, 10 and 50 mg L^{-1} groups were fixed in a mixture of 4% paraformaldehyde and 2% glutaraldehyde in 0.1 M sodium cacodylate buffered solution at pH 7.4. After several washes in the same buffer, samples were post-fixed in 1% OsO_4 for 1.5 h at 4 °C and then first dehydrated in a graded ethanol series followed by critical-point drying, using liquid CO_2 in a Balzers Unions CPD 020 apparatus (Balzers Unions, Lichtenstein). By using the stereomicroscope, the digestive systems have been dissected and separated from the remaining body portions, and processed as above. All samples for SEM analyses were mounted onto standard Aluminum stubs, gold sputtered and analyzed under a Zeiss LEO 1430 SEM at 20 kV.

Results

CNM physicochemical characterisation

The main results of the CNM physicochemical characterisation are available in Figure S1 (available in the online version of the paper) which shows for each NP: *i*) images of aggregates from the three selected CNMs by SEM (Fig. S1a); *ii*) their representative EDX spectra (Fig. S1b); *iii*) TEM images of as-prepared NPs (Fig. S1c); *iv*) NP size distributions of the suspensions (Fig. S1d); *v*) hydrodynamic size distribution from DLS measurements (Fig. S1e), and *vi*) results from PAH analyses (Fig. S1f). For clarity, results relative to each NP are reported separately below.

CNP

Figure S1a shows the typical round shape of CNP as observed by SEM. The EDX analyses confirmed the purity in carbon content of the used nanopowder: besides the little percentage of oxygen (due to the presence of surface oxides, (Boehm, 2002)), and of Cu (due to the used grids), only traces of Al and Si were present, these being however 0.16 and 0.42% of the total atomic percentage, respectively (Fig. S1b). CNP size distribution, performed on images taken by TEM (Fig. S1c), was mainly between 10 and 40 nm (80%), with only a small percentage exceeding 50 nm (9.0%); the mean particle diameter was 28.5±14.3 nm (Fig. S1d). CNP ζ-potential values were -10.6, -12.9 and -15.9 mV for 1, 10 and 50 mg L^{-1} suspensions, respectively. Measured values were slightly negative, with little differences among the concentrations, these likely deriving from the different aggregation status, while the small differences of the ζ-potential values from the point of zero charge accounted for the limited stability of the colloidal suspensions. The aggregation status was evaluated by measuring the hydrodynamic diameter as a function of the concentration over time. DLS analyses indicated an increase of the size of the aggregates both as a function of concentration and time. For the highest concentration (50 mg L^{-1}) at 24 h, the scattered light did not show any correlation profile, hampering the measurement of the diffusion coefficient, and consequently the estimation of the size of the aggregates (Fig. S1e). Measured PAHs concentration

in CNPs was 474 μg g^{-1} (ppm), as sum of 18 compounds, with pyrene (20%), benzo[g,h,i]-perylene (18%), indeno[1,2,3-cd]pyrene (16%) and fluoranthene (13%), as the most abundant ones, followed by benzo(b)fluoranthene+benzo(k)fluoranthene (9%) and acenaphtylene (7%) (Fig. S1f).

CNC

Images from both SEM and TEM clearly showed the cubic shape of CNC (Fig. S1a, c). The EDX analyses showed the presence of a little percentage of oxygen and Cu, together with traces of Al and Si (0.13 and 1.24% of the total atomic percentage, respectively) (Fig. S1b). CNC ζ-potentials values were lightly negative as for CNP (-12.0, -12.3 and -11.7 mV for 1, 10 and 50 mg L^{-1} suspensions, respectively), and very similar among them. DLS analyses indicated that the mean size of aggregates did not change over time at the lower concentrations (1 and 10 mg L^{-1}), lying in the range of 250-350 nm. Their dimensional distribution (side length) ranged between 6.6 nm and 349 nm and the typical wall thickness was 5.9 nm (Fig. S1d). Cubes were empty, some of them appeared to be broken or open at side or corner level. The hydrodynamic diameter at the highest concentration (50 mg L^{-1}) was higher and increased as a function of time (Fig. S1e). A more detailed characterization is available in (Marzorati, 2015). Total PAHs concentration in CNCs (sum of 18 compounds) was 1430 μg g^{-1} (ppm). PAH levels in CNCs were 3 and 5 times higher than in CNPs and CNTs, respectively, even if only few compounds were measured above the LOQs (in CNCs naphtalene and acenaphtylene accounted for 95% of the PAH sum) (Fig. S1f).

CNT

Images of CNT by SEM and TEM showed the typical tube shape of these NPs (Fig S1a, c). The EDX spectra showed the presence of a little percentage of oxygen and Cu, and traces of Na and Si (0.43 and 0.34% of the total atomic percentage) (Fig. S1b). While the supplier statement about the sizes was 6-12 nm in diameter and 2.5-20 μm in length, measured diameters ranged between 3.8 nm and 50 nm, with a mean thickness of 16.8 nm and a large variability in length because of CNT

susceptibility to be broken. The max measured length was about 7 μm (Fig. S1d). ζ-potentials were -10.1, -14.4 and -13.3 mV for 1, 10 and 50 mg L^{-1} suspensions, respectively. Measured values were slightly negative as for the others NPs and almost constant for the different concentrations. DLS analyses of MWCNTs confirmed their limited stability as colloidal suspensions, and already at the lower concentrations they settled, leaving a small fraction as suspended aggregates after 24 h, which poorly scattered light. At 10 and 50 mg L^{-1} the trend indicated an increase over time of the mean sizes of aggregates. At the higher concentration the extent of aggregation increased, forming fluctuating aggregates of about 1 μm (Fig. S1e). Total PAHs concentration (sum of 18 compounds) in CNTs was 265 μg g^{-1} (ppm). Among the studied NPs, CNTs showed the lowest PAH levels with acenaphtylene (38.6%) and benzo(a)pyrene (25.0%) as the most abundant compounds (Fig. S1f).

Acute toxicity

At the end of the exposure test, no mortality occurred in CNP and CNT control groups, and only one immobile daphnid was recorded in the controls of CNCs. In the test media, pH values were almost constant during the experiment (maximum differences between 0 and 48 h of 0.97, 0.63 and 0.34 pH units for CNPs, CNTs and CNCs, respectively). Oxygen content was always high and near saturation, varying between 8.84-10.1 mg L^{-1} (minimum-maximum interval at time 0) and 8.81-9.11 mg L^{-1} (minimum-maximum interval at 48 h). Both mortalities and physicochemical parameters met the OECD validity criteria (OECD, 2004). In the exposure experiments, the three used NPs showed a low level of toxicity, none of them reaching the Effective Concentration for 50% of the test population (EC_{50}), even at the highest concentrations. Anyway, a higher concentration range was not considered here for three reasons: *i*) the tested concentrations were already high (up to 50 mg L^{-1}), and higher concentrations would be nonsense; *ii*) the digestive systems of exposed daphnids were completely full with NPs, even at the lowest concentration (Fig. 1), and many aggregates were visible attached not only to the carapaces, but also inside them, and *iii*) the study of internalization pathways and possible effects at cellular level by microscopic analyses needed living

specimens.

Despite their low general toxicity, CNPs and CNCs presented time- and concentration-dependent toxicity, reaching the maximum of 35% immobilization in 50 mg L^{-1} CNP group and 20% lethality in 50 mg L^{-1} CNC group. Comparing the toxicities of these two CNMs however, CNCs resulted more toxic than CNP since they showed significant effects on daphnids from 10 mg L^{-1}, while the first effects observed in CNP were recorded in the 20mg L^{-1} group. Differently from CNPs and CNCs, CNTs did not present any significant immobilization or lethality effects at these concentrations.

Stereomicroscopic and histological analyses

Figure 1 shows the huge amount of carbon NPs ingested by daphnids during exposure: samples from all concentrations display evident black masses inside the digestive systems and within the thoracic appendages, specialized in filtering food particles from water. According to the observed effects on immobilization, NP accumulation into the gut and their presence upon the carapace was concentration-dependent. CNP and CNC samples appeared to be the most affected by NPs, their guts being completely full of black masses, while exposure to CNTs caused a lower intensity of NP inside gut and within appendages (Fig. 1G-L).

In *Daphnia* species, the thorax bears five pairs of leaf-like limbs, showing great variability in both shape and function (Mittmann *et al.*, 2014); according to the literature, epipodites are responsible for gas exchanges and ion homeostasis (Kikuchi, 1983, Goldmann *et al.*, 1999, Paul *et al.*, 2004, Maas, 2009). Because of these essential functions and since many aggregates from all NPs have been observed accumulating among these appendages, we addressed ultrastructural analyses also to these epithelia, called hereafter gills. Moreover, while gut is a very well known accumulation and entry site for NPs (Elder *et al.*, 2009, Bacchetta *et al.*, 2012, Bacchetta *et al.*, 2014, Santo *et al.*, 2014), gills of *D. magna* have not yet been studied from this point of view, making this investigation more interesting.

Figure 2 shows sagittal sections from both controls and exposed samples. *D. magna* gut is composed by a short anterior region, the *stomodeum* or foregut, which is protected by a thick chitin layer with the function of transferring food from the mouth to the actual gut. This one, called midgut has anteriorly two *diverticula* or hepatic *caeca*, and both have digestive and absorptive functions. The final portion of the gut is called hindgut and is involved in the reabsorption of liquids (Quaglia *et al.*, 1976). Microscopic analyses have been performed mainly focusing at the midgut region that is specifically involved in absorption. Contrary to controls, samples exposed to CNMs display large masses occupying the entire lumen of the gut (Fig. 2D-L). These masses entered into contact with the apical cell portions, and in the most affected fields they cause disruption of the peritrophic membranes, whose role in protecting epithelial cells from mechanical damages is thus overcome. While at low concentrations some gut regions seemed to be perfectly conserved, at the highest concentrations the final portion of the midgut appeared completely altered. In these cases the epithelium was extremely reduced, the brush border eroded, and cells showed large empty spaces among them and between them and the basal lamina. These morphologies were mainly diffused in the 50 mg L^{-1} groups for all the tested NPs.

Besides the digestive system, our analyses additionally considered the epithelial tissue of gills. Figure 3 shows the main feature of *D. magna* gills in control samples. Gills have an almost semi-spherical shape with an internal cavity, the hemolymphatic space, defined by a single layer of epithelial cells and, more externally, a thin cuticle (Fig. 3A). Two different cellular types compose the epithelium: the dark cells, important for osmoregulation, and the light cells, responsible for gas exchanges (Kikuchi, 1983). Due to the highly active metabolism, both cells display a high number of mitochondria, and also complex tubular systems, and cellular protrusions toward the inner cavity (Goldmann *et al.*, 1999, Smirnov, 2013) (Fig. 3B-F).

Histological sections from samples exposed to the three NPs occasionally showed black masses attached to the cuticle (Fig. 2K), but no evidences of NPs in the hemolymphatic spaces have been recorded (Fig. 3J-L). The epithelium maintains its integrity also at the highest concentrations at

which some morphological alterations appear in CNP treated samples; these mainly consist in the occurrence of large vacuoles and empty spaces, near the cuticle.

Morphological analyses by Scanning Electron Microscope (SEM)

The general morphology of daphnids, and some details from control samples are shown in Figure S2 (available in the online version of the paper). Figure 4 shows the midgut from control samples, in which the gut muscolaris, the peritrophic membrane and the microvilli are well visible (Fig. 4A-C). In particular, Fig. 4C shows the width of the intestinal wall and the presence of the thick brush border on the apical portion of the digestive cells. Figure 5 shows detailed portions of the midgut from samples exposed to the three selected NPs, in which the differently shaped CNMs are well recognizable. These images evidence also the huge mass of CNMs filling the gut, confirming the digestive system as a preferential accumulation site for all NPs. The ultrastructural analysis by TEM has been performed on the gut at this level.

Figure 4 additionally shows the general morphology of daphnids' epipodites, which appear like inflated smooth structures, attached to the thoracic limbs (Fig. 4D-F). According to the literature, epipodites are structures on the outer edge of the thoracic appendages serving as gills and for osmoregulation. They are inserted on the lateral edge of the limb base and their design ranges from being branched filaments to having a club-, lobe- or leaf-like shape (Maas, 2009). In controls, as well as in samples exposed to CNMs, epipodite I, II and III have a more complex architecture if compared to epipodite IV and V. Epipodite I is podgy and more rounded than epipodite II and III, which on the contrary are clearly bilobated and hearth-shaped. Epipodite IV and V appear more oblong, almost linear and undivided (Fig. 4D). The sizes of epipodites differ among them and range between 15 and 120 µm. Epipodite II and III are bigger than the others, reaching about 100-120 µm in both width and length, while epipodite V is the smallest, with a length of about 80 µm and a maximum width of 15-20 µm. No differences have been observed between controls and treated samples, except for the presence of few NPs near the epithelium of the exposed samples, but no

modification to in the morphology of their epipodites have been detected.

Interestingly, while looking at high magnification for a possible uptake of NPs through the cuticle, we found several holes spread on the outer surface of epipodites, without apparent order. These structures, indiscriminately present in both controls and exposed samples, have diameters that range between 65 and 150 nm, and are distributed all along the epipodites (Fig. 6). At first glance, they seem to be as numerous as the cells forming the epipodites, whose cellular borders are recognizable in the images taken by SEM. To our knowledge, they have never been reported in literature so far, and the physiological meaning, currently unknown, is now under study in our laboratory.

Ultrastructural analyses by Transmission Electron Microscope (TEM)

Figure 7 shows some fields from gut of controls by TEM displaying a regular epithelium composed by a single layer of cuboidal to columnar cells with a thick border of microvilli (Fig. 7A-B), an electron-dense cytoplasm rich in organelles, and a highly folded basal plasma membrane, separated from the gut muscolaris by a granular basement membrane (Fig. 7C-D).

As observed by light microscopy (Fig. 2D-L), the gut lumen from exposed samples appears full of NPs, together with residual membranes coming from digested food and/or peritrophic membrane disruptions. In none of the observed fields the peritrophic membranes appear integer and in the most affected fields, they are no more visible. Such a condition allows NPs to physically enter into contact with enterocytes (Fig. 8F, 9B, and 10A). All the three studied NPs have been observed above and among the microvilli, but also in the space between microvilli and the apical portion of the enterocytes (Fig. 8, 9 and 10). Additionally, CNPs and CNTs have been detected inside the digestive cells or in the paracellular spaces between them, and also in the smooth muscle tissue encircling the enterocytes, namely the gut muscolaris. Unlike CNTs, CNPs have been additionally observed into the numerous infoldings of the basal plasma membrane (Fig. 8C, E). No CNCs have ever been observed either into the digestive cells or in the underneath tissues (Fig. 9).

Looking to the effects observed in the enterocytes, many similarities exist among the three studied

NPs, but also some interesting differences. Exposures to CNP, CNC, and CNT were all able to cause: *i*) empty spaces between adjacent cells (Fig. 8E, 9A and 10C); *ii*) detachment of the digestive cells from the basal lamina (Fig. 8E-F, 9B-C, 10F), and *iii*) a high number of lamellar bodies and autophagy vacuoles in the cytoplasm (Fig. 8D, 9B-C, and 10D-E). Contrary to CNT, CNP and CNC additionally caused: *iv*) partial or complete dissolution of the brush border (Fig. 8F and 9B, D), and *v*) thinning of the digestive epithelium (Fig. 8F, 9B-C). Interestingly, while CNCs seem unable to be internalized by cells, they show the same cellular alterations described for CNPs. Indeed, at 1 mg L^{-1} samples exposed to CNCs do not show any pathological modification, but at 10 mg L^{-1} the observed effects are very similar to those detected in the 50 mg L^{-1} CNP exposed group.

As in the digestive cells, CNPs and CNTs have been detected in the epipodites (Fig. 11). Samples exposed to the lowest CNP concentration (1 mg L^{-1}) already showed some NPs in and between the epithelial cells of the epipodites, while the first CNTs have been detected in the samples exposed to 10 mg L^{-1}. While some CNTs were observed pierced into the cuticle (Fig. 11D), suggesting the outer layer of epipodites as the main entry route for these NPs, from our analyses we are still unable to discriminate the way CNPs used to enter into cells: via the cuticle or from the hemocoel.

Contrary to CNPs and CNTs, CNCs have never been observed into the epipodites, but like the other two CNMs they were able to determine the same effects in these structures (Fig. 12). In fact, all NPs caused: *i*) cellular disorganization; *ii*) empty spaces into the cytoplasm; *iii*) large autophagy vacuoles rich in lamellar structures; *iv*) great numbers of multivesicular bodies, MVB, and *v*) dilatation of the paracellular spaces. These effects have been observed starting from 1 and 10 mg L^{-1} after exposure to CNTs and CNCs, respectively. CNPs determined the same effects, but only at the highest concentration.

Discussion

Immobilisation and mortality data revealed a low acute toxicity for all the tested NPs with EC_{50} values >50 mg L^{-1}. These results disagree with data available in literature, at least for CNP and

CNT. For CNC, no toxicity data are available so far, and to our knowledge the present paper represents the first contribute to the acute toxicity of CNC in living systems and definitely in *D. magna*. On the contrary, CNP (mainly carbon black, CB) and CNT have already been studied not only in *D. magna*, but also in many other animal models, such as the green algae *Chlorella vulgaris* and *Pseudokirchneriella subcapitata* (Schwab *et al.*, 2011, Long *et al.*, 2012), the mussel *Mytilus galloprovincialis* (Canesi *et al.*, 2010), the cladoceran *Ceriodaphnia dubia* (Kennedy *et al.*, 2008), the fruit fly *Drosophila melanogaster* (Liu *et al.*, 2009), the amphibian *Xenopus laevis* (Mouchet *et al.*, 2010, Bacchetta *et al.*, 2012), the zebrafish *Danio rerio* (Asharani *et al.*, 2008), and the mouse (Magrez *et al.*, 2006, Pulskamp *et al.*, 2007). Toxicity data related to *D. magna* have been obtained for fullerene (Oberdorster *et al.*, 2006), graphene (Fan *et al.*, 2016), and mainly for CNT, for which an extensive literature is available (see reviews by (Petersen *et al.*, 2011, Jackson *et al.*, 2013, Boncel *et al.*, 2015)). Data reported for CNT vary greatly, depending on the experimental conditions: use of pure CNT, CNT stabilized with natural organic matter or grafted with polyethylenimine (Jackson *et al.*, 2013). Since our exposures were mainly planned for studying by a morphological approach the possible uptake routes and the cytotoxic mechanisms of CNT, we used pure CNT without any kind of stabilizer. A previous paper has already considered the toxicity of pristine CNT and reported ecotoxicological immobilization and mortality values, which however were higher than ours. In fact, Zhu and coworkers found EC_{50} and LC_{50} values of 8.7 and 22.8 mg L^{-1}, respectively (Zhu *et al.*, 2009), which differed from our results (>50 mg L^{-1}). Data related to CB in the bulk form are more similar to ours, being the estimated EC_{50} and LC_{50} values 37.6 and 61.6 mg L^{-1}, respectively. It is worth noting that Zhu et al. (Zhu *et al.*, 2009) maintained the test suspensions under constant agitation in order to reduce sedimentation, while in our experiment we did not. As already stated, our goals were mainly focused on the effects due to the morphology of CNM and not on establishing ecotoxicological thresholds. Indeed, also at the lowest concentrations the gut of samples exposed to our CNM resulted completely filled with NPs (Fig. 2), making a further stabilization of the suspensions a non-mandatory issue for our purposes.

Data from the literature confirm that *D. magna* can take up CNM from the exposure medium and that the intestine is the main organ by which the water flea accumulates CNM (Fan *et al.*, 2016). While NP accumulation into the digestive system is clearly understandable, less clear is the fate of the large amount of NM present inside it. In fact, while some paper reported that particles resistant to digestion may accumulate in the hindgut of *Daphnia* sp. when all other materials are digested (Lampert, 1987), and that starved animals can retain feces in the midgut indefinitely (Gophen, 1981) as well, there are strong evidences demonstrating that when specimens are provided with new food they can clear their gut from ingested materials (Gillis *et al.*, 2005). According to Kennedy et al. (Kennedy *et al.*, 2008), literature data would suggest that food ingestion was necessary for gut clearance. Indeed, after our exposures, surviving specimens not used for microscopic analyses were maintained at standard conditions and allowed to develop in culture medium, and interestingly they presented traces of black masses in the gut for at least 8-10 days, even if regularly fed. This disagrees with data from Edgington et al. (Edgington *et al.*, 2010) who, in a study on the toxicity of ingested CNT, reported a clearance time for *D. magna* as long as 28 h. We did not know if after this period our tested CNMs were still present inside the digestive system of *D. magna* (this issue was not considered in the present paper), but we speculated on the time CNM remained inside the gut and, consequently, into contact with the digestive epithelium. Certainly, daphnids eliminated with difficulty our CNM, and algae did not determine immediate gut clearance. A prolonged gut resident time represents an additional risk not only for the specimen itself, but also for the environment in general, considering that *D. magna* is one of the low trophic level organisms in the freshwater food chain. Data from the literature demonstrated that NPs were able to pass from the water column to the aquatic food web (Ferry *et al.*, 2009), and that engineered nanomaterials could be transferred to higher trophic organisms through dietary intake (Holbrook *et al.*, 2008). This suggests that a long residency time into the gut should be considered as a source of CNMs for higher trophic level. A low elimination capacity of daphnids introduces also the issue of the "physical" toxicity of these CNM, considering the longer period they stay into contact with the digestive epithelium. To this

regard it must be outlined that our ultrastructural analyses evidenced NP internalization into the digestive epithelium and the epithelial cells of the epipodites in CNP and CNT exposed samples, while for CNC no internalization was ever observed into these or other tissues. In the gut, CNP and CNT were found: *i*) among microvilli; *ii*) inside them; *iii*) free in the cytoplasm; *iv*) in the paracellular space, and *v*) at the basal lamina level (Fig. 8 and 10). In gills, they were observed at various levels into both dark and light cells (Fig. 11): mainly near the cuticle, but also close to the hemocoel. The finding of a single CNT across the cuticle, which seems to be piercing this layer (Fig. 11D), would suggest that at least CNTs were able to enter cells using this route, even if the uptake through the hemocoel could not be excluded. It is likely that NPs might use both routes, considering the reduced thickness (0.2-0.5 μm) of the epipodite cuticle (Kikuchi, 1983), and the known possibility for NM to translocate into the body cavity of *D. magna* (Scanlan *et al.*, 2013). Translocation of NM is widely reported in literature for *D. magna*, but also for other animal models and it is known for both metallic and carbonaceous NM (Oberdorster *et al.*, 2002, Elder *et al.*, 2009, Kreyling *et al.*, 2009, Bacchetta *et al.*, 2012, Scanlan *et al.*, 2013, Bacchetta *et al.*, 2014, Mattsson *et al.*, 2016). All these studies underline the possibility for NP to cause secondary effects in non-target organs and/or to produce detrimental effects during later developmental stages or even in the offspring of treated specimens. This indeed has already been reported for CB, which is known to cause secondary effects, such as spermatogenesis reduction in mouse (Yoshida *et al.*, 2009), as well as metabolic alteration in the offspring of mothers exposed to CB (Jackson *et al.*, 2012).

Together with the great amount of NP inside the gut in all the exposed samples, we also observed a concomitant lost of the peritrophic membrane (PM), that completely disappeared in the most affected fields, namely in the samples treated with the highest NP concentrations. Among the several functions attributed to PM, this structure acts as a protective layer for the digestive epithelium from possible pathogens (Peters, 1992). It is clear that a disruption of this layer allows NP to enter into contact with enterocytes, which are thus more subjected to the physical pressure exerted by them. Without PM, the brush borders first, and the apical cytoplasmic portion of the

digestive cells later, resulted more affected by the steric obstruction of NP, which are able to exert ruptures and damages via an "abrasion" effect. Considering the very similar chemical compositions of our tested NP (Fig. S1), one parameter that may rule NP penetration into cells and tissues is shape. Together with size, NP shape plays a key role in NP uptake, and several published papers have already underlined the importance of this factor (Gratton *et al.*, 2008, Elder *et al.*, 2009, Albanese *et al.*, 2012). Being completely different in shape (spherical, cubic and tubular), our tested NP would have determined different effects on tissues (gut and gills); indeed, looking at our results, we observed very similar effects on gut and gill cells after exposure to the three differently shaped NM. In fact, we observed for all NP: *i*) empty spaces between cells; *ii*) detachment of the enterocytes from the basal lamina, and *iii*) large number of lamellar bodies and autophagy vacuoles. It would seem that effects were independent from shape, at least for carbonaceous nanomaterials on gut and gills of *D. magna*. Interestingly the only NP that did not enter the cell (CNC) was observed to cause additional effect, namely partial or complete dissolution of the brush border and thinning of the digestive epithelium. These two findings well agree with the particular shape of CNC, whose edges can erode and exert abrasive actions of soft tissues more easily than spheres or nanotubes can do. Although unable to be internalized by cells, CNC were observed to dig at the microvilli level and at the apical cell portion, suggesting that a mere physical action is additionally performed by this kind of NP. Moreover, it must be outlined that edges and corner sites are considered particularly reactive (Kuech, 2016) and this would explain the higher toxicity of the cubic shape with respect to the remaining two.

It is known from the literature that interactions at the nano-bio interface can be either chemical or physical (Nel *et al.*, 2009), and that one of the possible consequences of the physical contact between NP and biologic membranes is their disruption. The paper by Lerueil et al. (Leroueil *et al.*, 2007) in fact, have demonstrated that physical disruption of membranes, with the consequent formation of holes and/or thinned regions, was due to the interactions between NP and lipids. Results from our ultrastructural analyses, which showed detachment of cells from the basal lamina,

enlargement of the paracellular spaces and large vacuoles inside the cytoplasm, well agree with these data. Also the high number of MVB, mainly in the gills of exposed samples, is in accordance with membrane disruption, considering that MVB are known to serve for destroying damaged proteins (Piper and Katzmann, 2007). Moreover, since phagocytosis is reported to represent one of the possible biological responses to NP-membrane physical interaction (Elsaesser and Howard, 2012), our findings of many autophagic vacuoles (AV) inside the cytoplasm of both digestive and gill cells were not surprising, also considering that autophagic dysfunction and vesicle accumulation has been reported following NP treatment and also after exposure to carbonaceous NM (Poland *et al.*, 2008). Our ultrastructural analyses by TEM identified many AV into tissues of exposed samples and sometimes empty vacuoles that were likely advanced or terminal developmental stages of the same AV. In all treated samples, even at the lowest exposure concentrations, autophagy resulted greatly induced by CNP, CNC and CNT evidencing the induction capacity of this cell defense mechanism for all these NM. This well agrees with data by Stern et al. (Stern *et al.*, 2012) who reported that several classes of NM might induce autophagy in different biological models. Our observed effects are also consistent with the paper by Zhang et al. (Zhang *et al.*, 2009) who reported fullerene-induced autophagy in HeLa cells, and the work by Tsukahara et al. (Tsukahara *et al.*, 2015), who studied the effects of MWCNT on human pulmonary cells *in vitro* and evidenced that MWCNT were able to induce: *i*) autophagosome formation, *ii*) activation of autophagy regulation genes, and *iii*) increase of autophagy vacuoles.

From our morphological observations and according to the existing literature, we can conclude that shape is an important factor for NP uptake, at least in the digestive and gill cells of *D. magna*, determining a higher internalization of spherical and tube shape, if compared to the cubic one. Looking at the effects at cellular level, shape does not seem to be involved in determining the kind of pathology; on the contrary, considering the abundance of malformations and their degree of severity it seems to play a key role, being the cubic shape more effective than others in determining physical damages and cellular degeneration. The presence and mainly the physical contact between

CNM and cell membrane were able to induce the formation of AV and MVB, as the cell response to membrane damages. It must also be considered that we have observed very similar effects in different cellular types, namely in enterocytes of the midgut and in light and dark cells of the epipodites, which although being both epithelial cells, they were specialized in very different functions. The presence of comparable effects in different cells/tissues suggest that the observed effects are independent from the cellular type, and that are linked to the nature of the NP itself. Such a hypothesis needs of course to be tested in order to better understand the real role of CNM in determining toxicity.

Acknowledgements

Authors wish to thank Dr. M. Ascagni, Università degli Studi di Milano for her help in the use of the ImageJ® software, and Prof. G. Melone, Università degli Studi di Milano, for his helpful advices.

Disclosure statement

The authors report no conflicts of interest

References

Albanese, A., Tang, P.S. & Chan, W.C.W., 2012. The Effect of Nanoparticle Size, Shape, and Surface Chemistry on Biological Systems. *Annual Review of Biomedical Engineering, Vol 14,* 14**,** 1-16.

Asharani, P.V., Serina, N.G., Nurmawati, M.H., Wu, Y.L., Gong, Z. & Valiyaveettil, S., 2008. Impact of multi-walled carbon nanotubes on aquatic species. *J Nanosci Nanotechnol,* 8**,** 3603-9.

Bacchetta, R., Maran, B., Marelli, M., Santo, N. & Tremolada, P., 2016. Role of soluble zinc in ZnO nanoparticle cytotoxicity in Daphnia magna: A morphological approach. *Environ Res,* 148**,** 376-385.

Bacchetta, R., Moschini, E., Santo, N., Fascio, U., Del Giacco, L., Freddi, S., Camatini, M. & Mantecca, P., 2014. Evidence and uptake routes for Zinc oxide nanoparticles through the gastrointestinal barrier in Xenopus laevis. *Nanotoxicology,* 8**,** 728-744.

Bacchetta, R., Santo, N., Fascio, U., Moschini, E., Freddi, S., Chirico, G., Camatini, M. & Mantecca, P., 2012. Nano-sized CuO, TiO(2) and ZnO affect Xenopus laevis development. *Nanotoxicology,* 6**,** 381-398.

Bacchetta, R., Santo, N., Marelli, M., Nosengo, G. & Tremolada, P., 2017. Chronic toxicity effects of ZnSO4 and ZnO nanoparticles in Daphnia magna. *Environ Res,* 152**,** 128-140.

Boehm, H.P., 2002. Surface oxides on carbon and their analysis: a critical assessment. *Carbon,* 40**,** 145-149.

Boncel, S., Kyziol-Komosinska, J., Krzyzewska, I. & Czupiol, J., 2015. Interactions of carbon nanotubes with aqueous/aquatic media containing organic/inorganic contaminants and selected organisms of aquatic ecosystems--A review. *Chemosphere,* 136**,** 211-21.

Canesi, L., Fabbri, R., Gallo, G., Vallotto, D., Marcomini, A. & Pojana, G., 2010. Biomarkers in Mytilus galloprovincialis exposed to suspensions of selected nanoparticles (Nano carbon black, C60 fullerene, Nano-TiO2, Nano-SiO2). *Aquat Toxicol,* 100**,** 168-77.

Chithrani, B.D. & Chan, W.C., 2007. Elucidating the mechanism of cellular uptake and removal of protein-coated gold nanoparticles of different sizes and shapes. *Nano Lett,* 7**,** 1542-50.

De Volder, M.F., Tawfick, S.H., Baughman, R.H. & Hart, A.J., 2013. Carbon nanotubes: present and future commercial applications. *Science,* 339**,** 535-9.

Edgington, A.J., Petersen, E.J., Herzing, A.A., Podila, R., Rao, A. & Klaine, S.J., 2014. Microscopic investigation of single-wall carbon nanotube uptake by Daphnia magna. *Nanotoxicology,* 8 Suppl 1**,** 2-10.

Edgington, A.J., Roberts, A.P., Taylor, L.M., Alloy, M.M., Reppert, J., Rao, A.M., Mao, J. & Klaine, S.J., 2010. The influence of natural organic matter on the toxicity of multiwalled carbon nanotubes. *Environ Toxicol Chem,* 29**,** 2511-8.

Elder, A., Vidyasagar, S. & Delouise, L., 2009. Physicochemical factors that affect metal and metal oxide nanoparticle passage across epithelial barriers. *Wiley Interdisciplinary Reviews-Nanomedicine and Nanobiotechnology,* 1**,** 434-450.

Elsaesser, A. & Howard, C.V., 2012. Toxicology of nanoparticles. *Adv Drug Deliv Rev,* 64**,** 129-37.

Fan, W.H., Liu, Y.Y., Xu, Z.Z., Wang, X.R., Li, X.M. & Luo, S.L., 2016. The mechanism of chronic toxicity to Daphnia magna induced by graphene suspended in a water column. *Environmental Science-Nano,* 3**,** 1405-1415.

Ferry, J.L., Craig, P., Hexel, C., Sisco, P., Frey, R., Pennington, P.L., Fulton, M.H., Scott, I.G., Decho, A.W., Kashiwada, S., Murphy, C.J. & Shaw, T.J., 2009. Transfer of gold nanoparticles from the water column to the estuarine food web. *Nat Nanotechnol,* 4**,** 441-4.

Frey, D., 1982. Contrasting strategies of gamogenesis in northern and southern populations of cladocera. *Ecology* 63**,** 19.

George, S., Lin, S., Ji, Z., Thomas, C.R., Li, L., Mecklenburg, M., Meng, H., Wang, X., Zhang, H., Xia, T., Hohman, J.N., Lin, S., Zink, J.I., Weiss, P.S. & Nel, A.E., 2012. Surface defects on plate-shaped silver nanoparticles contribute to its hazard potential in a fish gill cell line and zebrafish embryos. *ACS Nano,* 6**,** 3745-59.

Gillis, P.L., Chow-Fraser, P., Ranville, J.F., Ross, P.E. & Wood, C.M., 2005. Daphnia need to be gut-cleared too: the effect of exposure to and ingestion of metal-contaminated sediment on the gut-clearance patterns of D. magna. *Aquat Toxicol,* 71**,** 143-54.

Goldmann, T., Becher, B., Wiedorn, K.H., Pirow, R., Deutschbein, M.E., Vollmer, E. & Paul, R.J., 1999. Epipodite and fat cells as sites of hemoglobin synthesis in the branchiopod crustacean Daphnia magna. *Histochem Cell Biol,* 112**,** 335-9.

Gophen, M.G., B., 1981. The use of inorganic substances to stimulate gut evacuation in Daphnia magna. *Hydrobiologia,* 80**,** 3.

Gratton, S.E., Ropp, P.A., Pohlhaus, P.D., Luft, J.C., Madden, V.J., Napier, M.E. & Desimone, J.M., 2008. The effect of particle design on cellular internalization pathways. *Proc Natl Acad Sci U S A,* 105**,** 11613-8.

Handy, R.D., Henry, T.B., Scown, T.M., Johnston, B.D. & Tyler, C.R., 2008. Manufactured nanoparticles: their uptake and effects on fish--a mechanistic analysis. *Ecotoxicology,* 17**,** 396-409.

Hao, L., Chen, L., Hao, J. & Zhong, N., 2013. Bioaccumulation and sub-acute toxicity of zinc oxide nanoparticles in juvenile carp (Cyprinus carpio): a comparative study with its bulk counterparts. *Ecotoxicol Environ Saf,* 91**,** 52-60.

Holbrook, R.D., Murphy, K.E., Morrow, J.B. & Cole, K.D., 2008. Trophic transfer of nanoparticles in a simplified invertebrate food web. *Nat Nanotechnol,* 3**,** 352-5.

Hua, J., Vijver, M.G., Richardson, M.K., Ahmad, F. & Peijnenburg, W.J., 2014. Particle-specific toxic effects of differently shaped zinc oxide nanoparticles to zebrafish embryos (Danio rerio). *Environ Toxicol Chem,* 33**,** 2859-68.

Huang, Z., Geyer, N., Werner, P., De Boor, J. & Gosele, U., 2011. Metal-assisted chemical etching of silicon: a review. *Adv Mater,* 23**,** 285-308.

Ispas, C., Andreescu, D., Patel, A., Goia, D.V., Andreescu, S. & Wallace, K.N., 2009. Toxicity and developmental defects of different sizes and shape nickel nanoparticles in zebrafish. *Environ Sci Technol,* 43**,** 6349-56.

Jackson, P., Hougaard, K.S., Vogel, U., Wu, D., Casavant, L., Williams, A., Wade, M., Yauk, C.L., Wallin, H. & Halappanavar, S., 2012. Exposure of pregnant mice to carbon black by intratracheal instillation: toxicogenomic effects in dams and offspring. *Mutat Res,* 745**,** 73-83.

Jackson, P., Jacobsen, N.R., Baun, A., Birkedal, R., Kuhnel, D., Jensen, K.A., Vogel, U. & Wallin, H., 2013. Bioaccumulation and ecotoxicity of carbon nanotubes. *Chem Cent J,* 7**,** 154.

Kennedy, A.J., Hull, M.S., Steevens, J.A., Dontsova, K.M., Chappell, M.A., Gunter, J.C. & Weiss, C.A., Jr., 2008. Factors influencing the partitioning and toxicity of nanotubes in the aquatic environment. *Environ Toxicol Chem,* 27**,** 1932-41.

Khanna, P., Ong, C., Bay, B.H. & Baeg, G.H., 2015. Nanotoxicity: An Interplay of Oxidative Stress, Inflammation and Cell Death. *Nanomaterials (Basel),* 5**,** 1163-1180.

Kikuchi, S., 1983. The fine structure of the gill epithelium of a fresh-water flea, Daphnia magna (Crustacea: Phyllopoda) and changes associated with acclimation to various salinities. I. Normal fine structure. *Cell Tissue Res,* 229**,** 253-68.

Kim, K.T., Edgington, A.J., Klaine, S.J., Cho, J.W. & Kim, S.D., 2009. Influence of multiwalled carbon nanotubes dispersed in natural organic matter on speciation and bioavailability of copper. *Environ Sci Technol,* 43**,** 8979-84.

Kreyling, W.G., Semmler-Behnke, M., Seitz, J., Scymczak, W., Wenk, A., Mayer, P., Takenaka, S. & Oberdorster, G., 2009. Size dependence of the translocation of inhaled iridium and carbon nanoparticle aggregates from the lung of rats to the blood and secondary target organs. *Inhal Toxicol,* 21 Suppl 1**,** 55-60.

Kuech, T.R.H., R.J.; Pedersen, J.A., 2016. *Engineered nanoparticles and the environment: biophysicochemical processes and toxicity*: John Wiley & Sons, Inc. Hoboken, New Jersey.

Lampert, W., 1987. *Feeding and nutrition in Daphnia*: Memorie dell'Istituto Italiano di Idrobiologia dott. Marco de Marchi.

Leroueil, P.R., Hong, S.Y., Mecke, A., Baker, J.R., Orr, B.G. & Holl, M.M.B., 2007. Nanoparticle interaction with biological membranes: Does nanotechnology present a janus face? *Accounts of Chemical Research,* 40**,** 335-342.

Liu, X., Vinson, D., Abt, D., Hurt, R.H. & Rand, D.M., 2009. Differential toxicity of carbon nanomaterials in Drosophila: larval dietary uptake is benign, but adult exposure causes locomotor impairment and mortality. *Environ Sci Technol,* 43**,** 6357-63.

Long, Z., Ji, J., Yang, K., Lin, D. & Wu, F., 2012. Systematic and quantitative investigation of the mechanism of carbon nanotubes' toxicity toward algae. *Environ Sci Technol,* 46**,** 8458-66.

Lovern, S.B. & Klaper, R., 2006. Daphnia magna mortality when exposed to titanium dioxide and fullerene (C-60) nanoparticles. *Environmental Toxicology and Chemistry,* 25**,** 1132-1137.

Maas, A.H., C.; Haug, J.; Olesen, J.; Zhang, X.; Waloszek, D., 2009. Early crustacean evolution and the appearance of epipodites and gills. *Arthropod systematics & phylogeny,* 67**,** 19.

Magrez, A., Kasas, S., Salicio, V., Pasquier, N., Seo, J.W., Celio, M., Catsicas, S., Schwaller, B. & Forro, L., 2006. Cellular toxicity of carbon-based nanomaterials. *Nano Lett,* 6**,** 1121-5.

Marzorati, S., 2015. Pt-free nano- and micro-structured carbons for electrochemical oxygen reduction reaction. PhD Thesis. Università degli Studi di Milano.

Mattsson, K., Adolfsson, K., Ekvall, M.T., Borgstrom, M.T., Linse, S., Hansson, L.A., Cedervall, T. & Prinz, C.N., 2016. Translocation of 40 nm diameter nanowires through the intestinal epithelium of Daphnia magna. *Nanotoxicology,* 10**,** 1160-7.

Mittmann, B., Ungerer, P., Klann, M., Stollewerk, A. & Wolff, C., 2014. Development and staging of the water flea Daphnia magna (Straus, 1820; Cladocera, Daphniidae) based on morphological landmarks. *Evodevo,* 5**,** 12.

Mouchet, F., Landois, P., Puech, P., Pinelli, E., Flahaut, E. & Gauthier, L., 2010. Carbon nanotube ecotoxicity in amphibians: assessment of multiwalled carbon nanotubes and comparison with double-walled carbon nanotubes. *Nanomedicine (Lond),* 5**,** 963-74.

Nel, A.E., Madler, L., Velegol, D., Xia, T., Hoek, E.M.V., Somasundaran, P., Klaessig, F., Castranova, V. & Thompson, M., 2009. Understanding biophysicochemical interactions at the nano-bio interface. *Nature Materials,* 8**,** 543-557.

Oberdorster, E., 2004. Manufactured nanomaterials (fullerenes, C60) induce oxidative stress in the brain of juvenile largemouth bass. *Environ Health Perspect,* 112**,** 1058-62.

Oberdorster, E., Zhu, S.Q., Blickley, T.M., Mcclellan-Green, P. & Haasch, M.L., 2006. Ecotoxicology of carbon-based engineered nanoparticles: Effects of fullerene (C-60) on aquatic organisms. *Carbon,* 44**,** 1112-1120.

Oberdorster, G., Sharp, Z., Atudorei, V., Elder, A., Gelein, R., Lunts, A., Kreyling, W. & Cox, C., 2002. Extrapulmonary translocation of ultrafine carbon particles following whole-body inhalation exposure of rats. *J Toxicol Environ Health A,* 65**,** 1531-43.

Oecd, 2004. *OECD Guidelines for the Testing of Chemicals/Section 2: Effects on Biotic Systems, Test no. 202: Daphnia sp. Acute Immobilisation Test*: OECD Publishing.

Oecd, 2010. *Guidance manual for the testing of manufactured nanomaterials: OECD sponsorship programme.*: OECD Publishing.

Oecd, 2012. *Test No. 211: Daphnia magna Reproduction Test*: OECD Publishing.

Paul, R.J., Zeis, B., Lamkemeyer, T., Seidl, M. & Pirow, R., 2004. Control of oxygen transport in the microcrustacean Daphnia: regulation of haemoglobin expression as central mechanism of adaptation to different oxygen and temperature conditions. *Acta Physiol Scand,* 182**,** 259-75.

Peters, W., 1992. *Peritrophic Membranes* Berlin.: Springer-Verlag.

Petersen, E.J., Zhang, L., Mattison, N.T., O'carroll, D.M., Whelton, A.J., Uddin, N., Nguyen, T., Huang, Q., Henry, T.B., Holbrook, R.D. & Chen, K.L., 2011. Potential release pathways, environmental fate, and ecological risks of carbon nanotubes. *Environ Sci Technol,* 45**,** 9837-56.

Piper, R.C. & Katzmann, D.J., 2007. Biogenesis and function of multivesicular bodies. *Annu Rev Cell Dev Biol,* 23**,** 519-47.

Poland, C.A., Duffin, R., Kinloch, I., Maynard, A., Wallace, W.A., Seaton, A., Stone, V., Brown, S., Macnee, W. & Donaldson, K., 2008. Carbon nanotubes introduced into the abdominal cavity of mice show asbestos-like pathogenicity in a pilot study. *Nat Nanotechnol,* 3**,** 423-8.

Pulskamp, K., Diabate, S. & Krug, H.F., 2007. Carbon nanotubes show no sign of acute toxicity but induce intracellular reactive oxygen species in dependence on contaminants. *Toxicol Lett,* 168**,** 58-74.

Quaglia, A., Sabelli, B. & Villani, L., 1976. Studies on the intestine of Daphnidae (Crustacea, Cladocera) ultrastructure of the midgut of Daphnia magna and Daphnia obtusa. *Journal of Morphology,* 150**,** 711-725.

Roberts, A.P., Mount, A.S., Seda, B., Souther, J., Qiao, R., Lin, S., Ke, P.C., Rao, A.M. & Klaine, S.J., 2007. In vivo biomodification of lipid-coated carbon nanotubes by Daphnia magna. *Environ Sci Technol,* 41**,** 3025-9.

Sanchis, J., Olmos, M., Vincent, P., Farre, M. & Barcelo, D., 2016. New Insights on the Influence of Organic Co-Contaminants on the Aquatic Toxicology of Carbon Nanomaterials. *Environ Sci Technol,* 50**,** 961-9.

Santo, N., Fascio, U., Torres, F., Guazzoni, N., Tremolada, P., Bettinetti, R., Mantecca, P. & Bacchetta, R., 2014. Toxic effects and ultrastructural damages to Daphnia magna of two differently sized ZnO nanoparticles: Does size matter? *Water Research,* 53**,** 339-350.

Scanlan, L.D., Reed, R.B., Loguinov, A.V., Antczak, P., Tagmount, A., Aloni, S., Nowinski, D.T., Luong, P., Tran, C., Karunaratne, N., Pham, D., Lin, X.X., Falciani, F., Higgins, C.P., Ranville, J.F., Vulpe, C.D. & Gilbert, B., 2013. Silver nanowire exposure results in internalization and toxicity to Daphnia magna. *ACS Nano,* 7**,** 10681-94.

Schneider, C.A., Rasband, W.S. & Eliceiri, K.W., 2012. NIH Image to ImageJ: 25 years of image analysis. *Nature Methods,* 9**,** 671-675.

Schwab, F., Bucheli, T.D., Lukhele, L.P., Magrez, A., Nowack, B., Sigg, L. & Knauer, K., 2011. Are carbon nanotube effects on green algae caused by shading and agglomeration? *Environ Sci Technol,* 45**,** 6136-44.

Shaw, B.J. & Handy, R.D., 2011. Physiological effects of nanoparticles on fish: A comparison of nanometals versus metal ions. *Environment International,* 37**,** 1083-1097.

Skjolding, L.M., Kern, K., Hjorth, R., Hartmann, N., Overgaard, S., Ma, G., Veinot, J.G. & Baun, A., 2014. Uptake and depuration of gold nanoparticles in Daphnia magna. *Ecotoxicology,* 23**,** 1172-83.

Smirnov, N., 2013. *Physiology of the Cladocera,* First Edition ed.: Academic Press.

Stern, S.T., Adiseshaiah, P.P. & Crist, R.M., 2012. Autophagy and lysosomal dysfunction as emerging mechanisms of nanomaterial toxicity. *Part Fibre Toxicol,* 9**,** 20.

Tsukahara, T., Matsuda, Y. & Haniu, H., 2015. The Role of Autophagy as a Mechanism of Toxicity Induced by Multi-Walled Carbon Nanotubes in Human Lung Cells. *International Journal of Molecular Sciences,* 16**,** 40-48.

Yoshida, S., Hiyoshi, K., Ichinose, T., Takano, H., Oshio, S., Sugawara, I., Takeda, K. & Shibamoto, T., 2009. Effect of nanoparticles on the male reproductive system of mice. *Int J Androl,* 32**,** 337-42.

Zhang, Q., Yang, W., Man, N., Zheng, F., Shen, Y., Sun, K., Li, Y. & Wen, L.P., 2009. Autophagy-mediated chemosensitization in cancer cells by fullerene C60 nanocrystal. *Autophagy,* 5**,** 1107-17.

Zhu, S., Oberdorster, E. & Haasch, M.L., 2006. Toxicity of an engineered nanoparticle (fullerene, C60) in two aquatic species, Daphnia and fathead minnow. *Mar Environ Res,* 62 Suppl**,** S5-9.

Zhu, X.S., Zhu, L., Chen, Y.S. & Tian, S.Y., 2009. Acute toxicities of six manufactured nanomaterial suspensions to Daphnia magna. *Journal of Nanoparticle Research,* 11**,** 67-75.

Captions to Supplementary Figures

Figure S1. Characterization of CNP, CNC, and CNT. (**a**) Images of NP aggregates by SEM. (**b**) EDX spectra from CNP, CNC, and CNT samples. (**c**) Images of NP aggregates by TEM. (**d**) Size frequency distributions of the tested CNM. (**e**) Variations of the average values of the CNM hydrodynamic diameters over time (24 h). (**f**) Results of PAH analysis.

Figure S2. Images of 48 h old *D. magna* specimens by SEM. **A**, whole body, low magnification. **B**, detail of the head region. **C**, the filtering apparatus of *D. magna*. **D**, detail of the abdominal region. White arrowhead = first antenna; black arrowhead = second antenna; white asterisk = apical spine; white arrow = mouth; black arrow = anus; black asterisk = post abdominal claw.

Figure S3. Elemental Spectroscopy Imaging (ESI) in samples of gut and gills exposed to 1 and 10 mg L^{-1} CNP. Carbon distribution is pseudocolored in red.

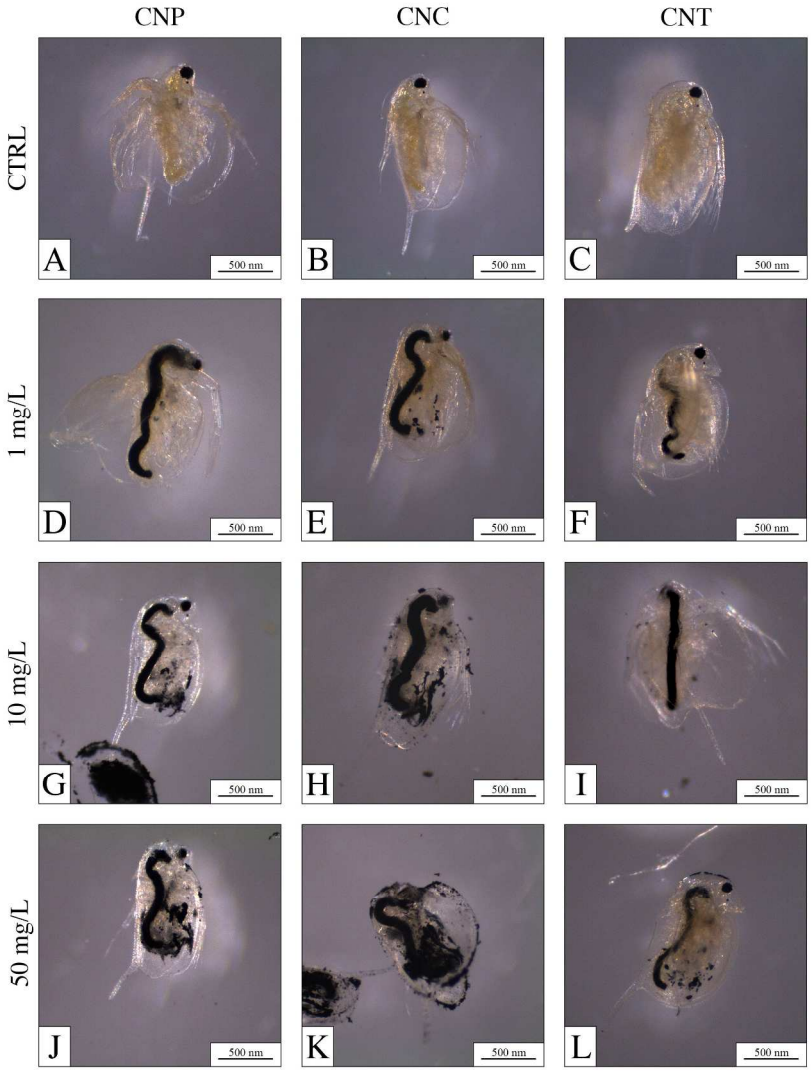

Figure 1. Stereomicroscopic images from 48 h old daphnids. (A-C) controls. (D-L) samples exposed to CNP, CNC and CNT showing their digestive tract full of NP.

209x297mm (300 x 300 DPI)

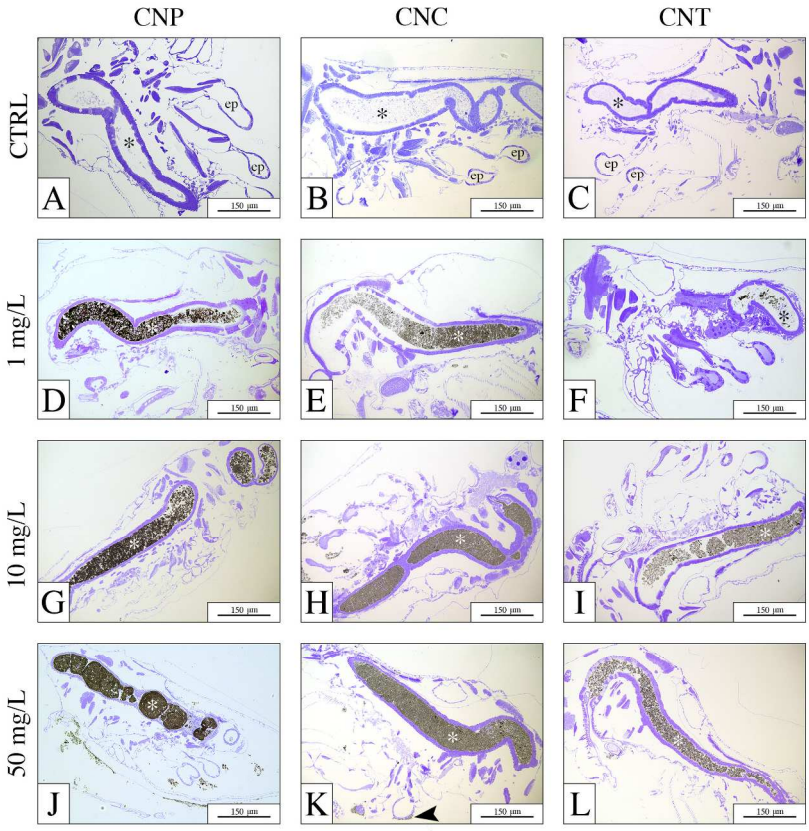

Figure 2. Semithin sections from control (A-C) and CNP, CNC and CNT exposed samples (D-L) showing the general anatomy of 48 h old daphnids. Sagittal sections from exposed samples show their digestive system engulfed by NP. * = gut lumen; ep = epipodite.

209x297mm (300 x 300 DPI)

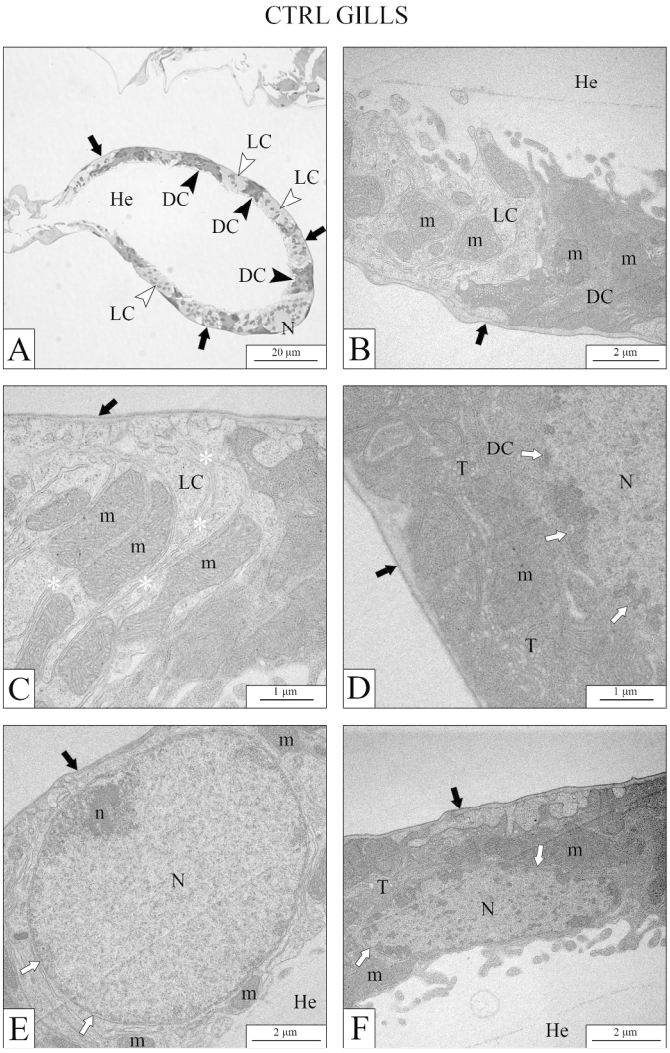

Figure 3. Microscopic images of gills from control daphnids. (A) Semithin cross section (0.7 µm) of an epipodite. (B-F) TEM images of the gill epithelium. He = Hemocoel; DC = Dark Cell; LC = Light Cell; N = Nucleus; m = mitochondrion; black arrow = cuticle; white asterisk = lateral plasma membrane; T = tubules; white arrow = nuclear envelope; n = nucleolus.

209x297mm (300 x 300 DPI)

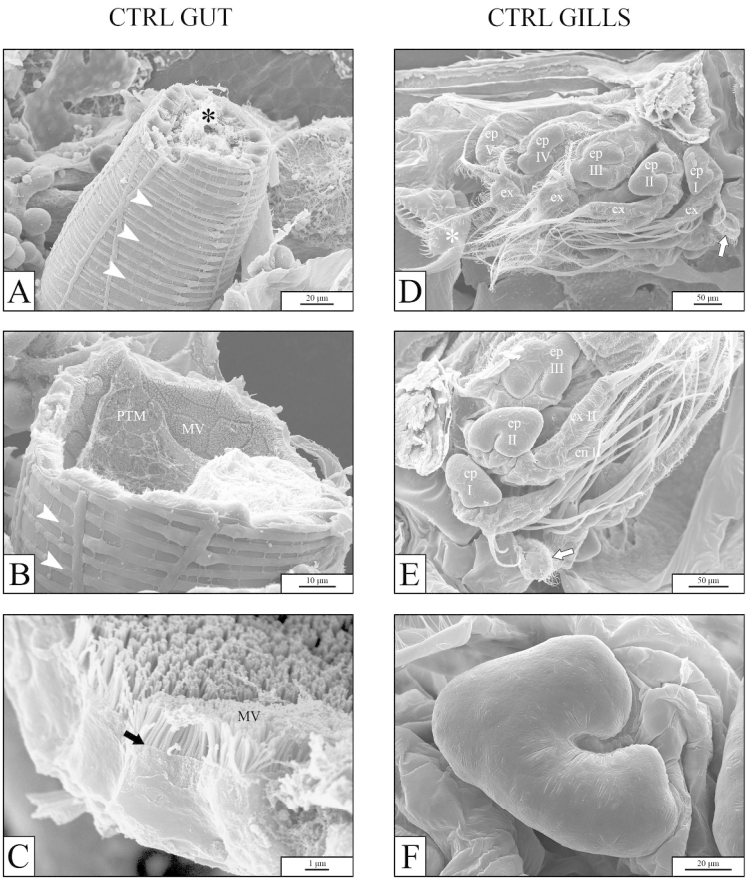

Figure 4. SEM images of gut (A-C) and gills (D-F) from control daphnids. (A) Low magnification of the gut with a visible gut muscolaris. (B) Medium magnification of the gut showing the lumen and the peritrophic membrane. (C) Detail of the digestive epithelium with a well developed brush border. (D) Lateral view of a daphnid showing its thoracic appendages. (E) Medium magnification of the first thoracic appendages. (F) Detail of epipodite III. White arrowhead = gut muscolaris; ep = epipodite; ex = exopodite; white arrow = mouth; PTM = peritrophic membrane; MV = microvilli; en = endite; black arrow = apical portion of the digestive cell.

209x297mm (300 x 300 DPI)

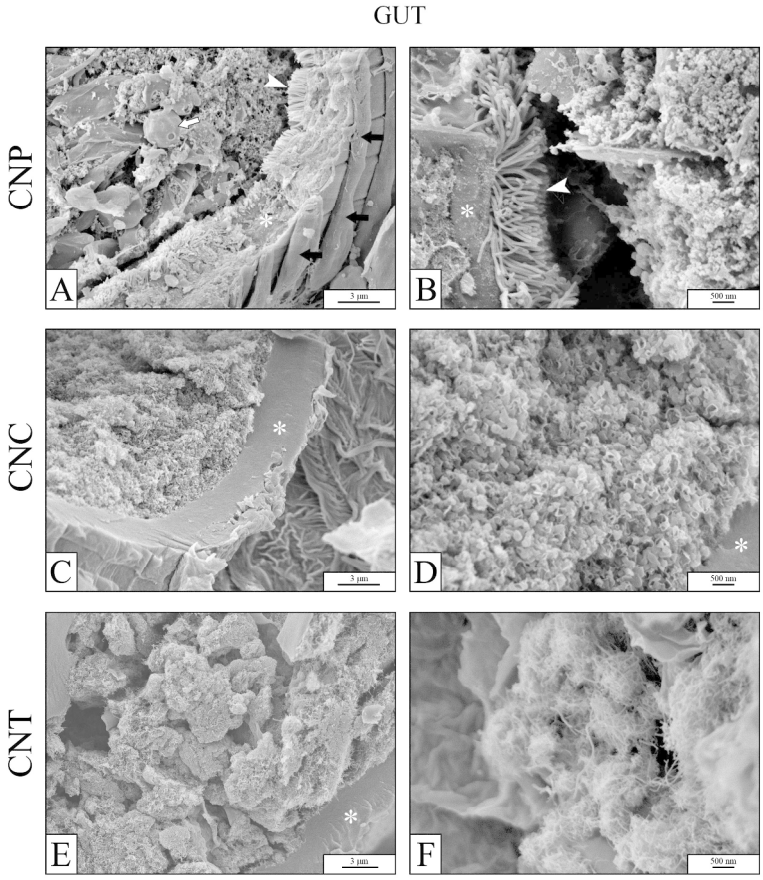

Figure 5. SEM images of the midgut from daphnids exposed to CNP (A-B), CNC (C-D) and CNT (E-F), showing large CNM amounts into the lumen. White arrow = yeast; white arrowhead = microvilli; black arrow = gut muscolaris; white asterisk = intestinal wall.

209x297mm (300 x 300 DPI)

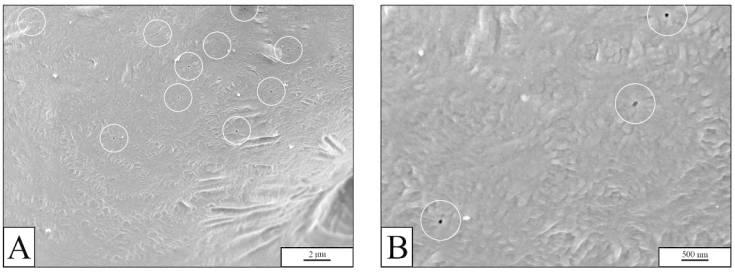

Figure 6. SEM images of an epipodite from a control sample. (A) Medium and (B) high magnification of the outer surface, showing the presence of several holes (white circle).

209x297mm (300 x 300 DPI)

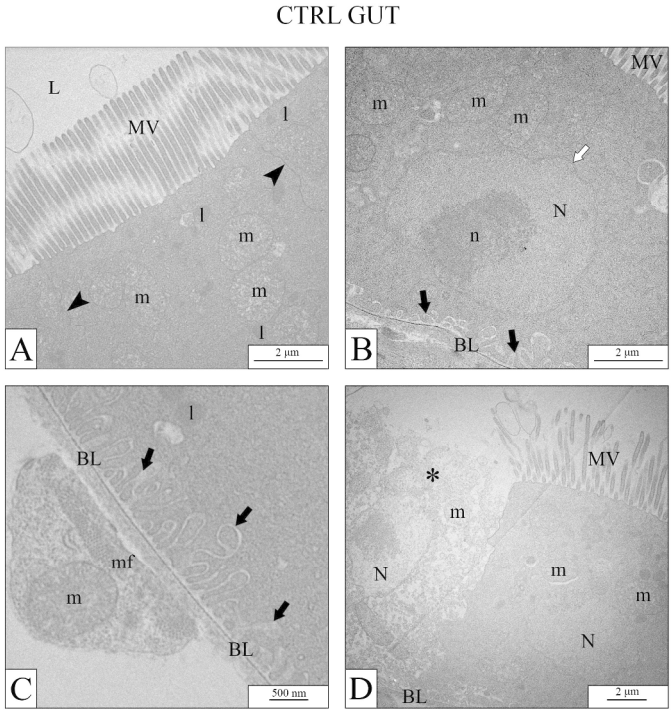

Figure 7. TEM images of the midgut from control samples showing the general architecture of the enterocytes. (A) Apical cell portion with a well-developed brush border. (B) A whole cell with a characteristic nucleus and an evident nucleolus. (C) Detail of the basal plasma membrane and, externally, of the gut muscularis. (D) Secretory cell near a regular enterocyte. L = gut lumen; MV = microvilli; l = lysosome; m = mitochondrion; black arrowhead = lateral plasma membrane; black arrow = basament plasma membrane; N = nucleus; n = nucleolus; BL = basal lamina; mf = myofibrils; * = secretory cell.

209x297mm (300 x 300 DPI)

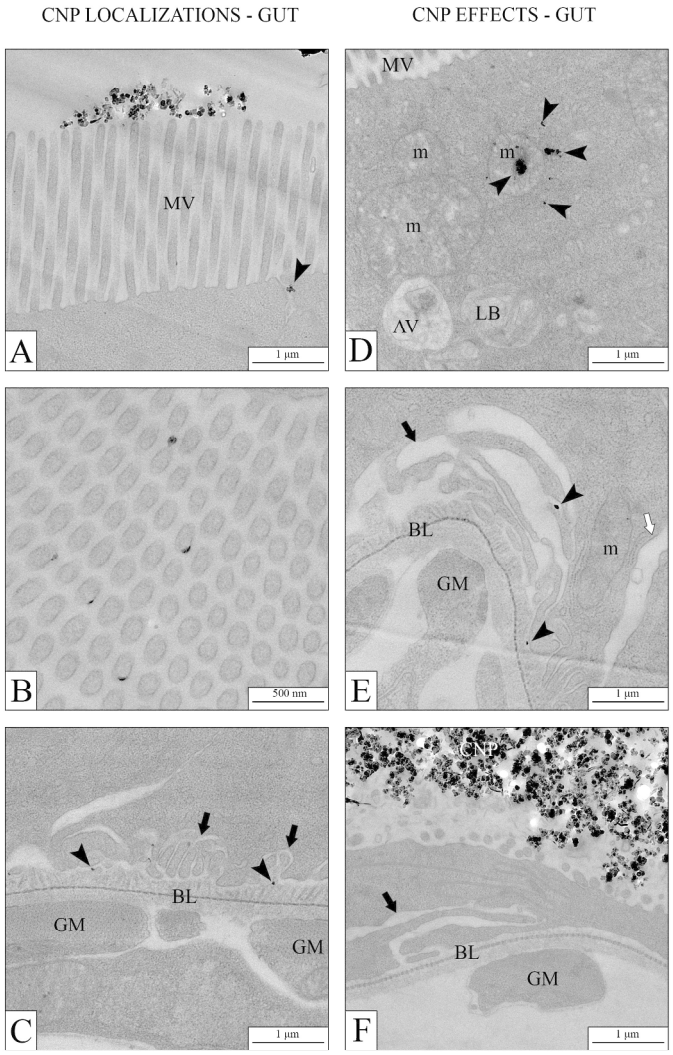

Figure 8. TEM images of the midgut from samples exposed to CNP, showing different NP localization (A-C) and the effects due to the exposure (D-F). (A) Longitudinal section of the apical cell portion of an enterocyte, showing some NP attached to the distal side of the brush border and a few NP into the space between two adjacent cells. (B) Transversal section of some microvilli with NP among them and also bound to their membranes. (C) Basal portion of an enterocyte showing some NP at the basement membrane level. (D) An autophagy vacuole and a lamellar body into the cytoplasm of an enterocyte where some NP aggregate are also visible. (E) Detail of the basal portion of an enterocyte with large empty spaces near the basal lamina. (F) Thinning of the digestive epithelium. MV = microvilli; black arrowhead = NP aggregate; m = mitochondrion; AV = autophagy vacuole; LB = lamellar body; black arrow = dilation of the spaces at the basement membrane level; BL = basal lamina; GM = gut muscolaris; white arrow = dilation of the lateral plasma membrane.

209x297mm (300 x 300 DPI)

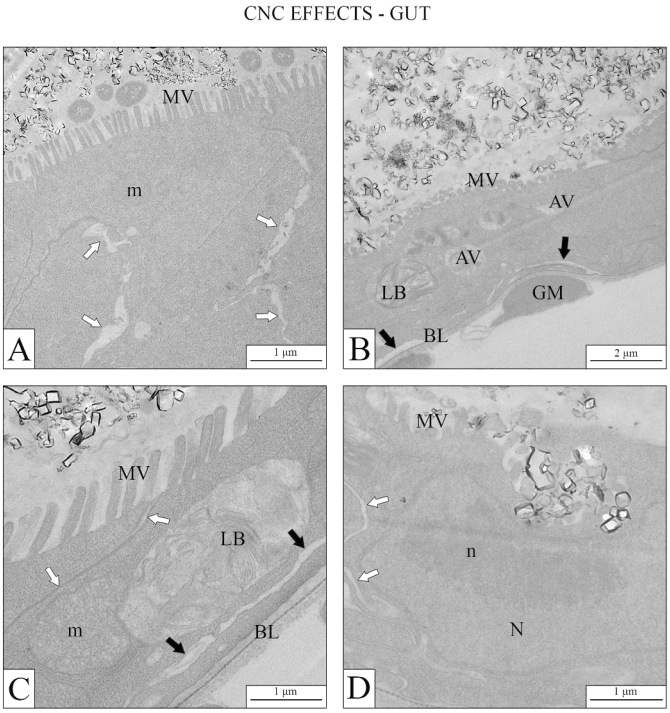

Figure 9. TEM images of the midgut from samples exposed to CNC, showing the effects due to the exposure. (A) Cells showing dilation of the paracellular spaces. (B) Low magnification of a very thin digestive epithelium. (C) Detail of a large lamellar body occupying the whole width of the enterocyte. (D) A digestive cell with some CNC digging its apical portion toward the nuclear envelope. MV = microvilli; m = mitochondrion; white arrow = paracellular spaces; AV = autophagy vacuole; LB = lamellar body; BL = basal lamina; black arrow = dilation of the spaces at the basement membrane level; N = nucleus; n = nucleolus.

209x297mm (300 x 300 DPI)

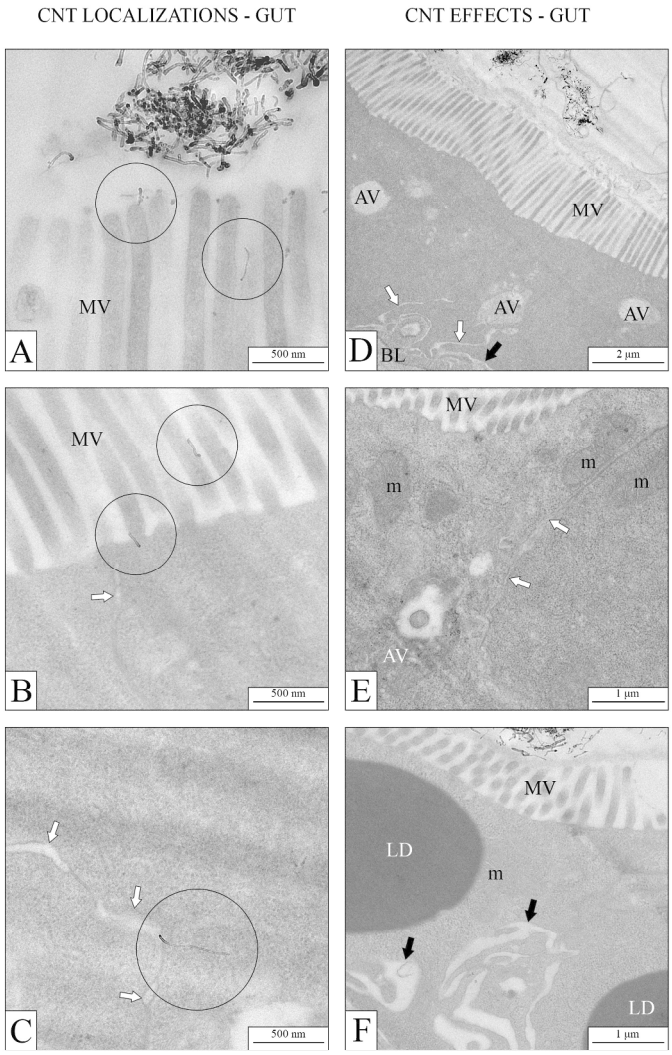

Figure 10. TEM images of the midgut from samples exposed to CNT, showing different NP localization (A-C) and the effects due to the exposure (D-F). (A) Cluster of CNT in the gut lumen and detail of some microvilli with a CNT among them and another one stinging the distal portion of a microvillus. (B) Detail of the apical portion of a digestive cell with one CNT between two adjacent microvilli and another one partially piercing the apical cell portion. (C) Detail of a CNT free in the cytoplasm. (D) Numerous autophagy vacuoles spread into the cytoplasm. (E) Detail of an autophagy vacuole. (F) Dilation of the spaces at the basal plasma membrane level. MV = microvilli; AV = autophagy vacuole; BL = basal lamina; white arrow = paracellular spaces; black arrow = dilation of the spaces at the basement membrane level; m = mitochondrion; LD = lipid droplet.

209x297mm (300 x 300 DPI)

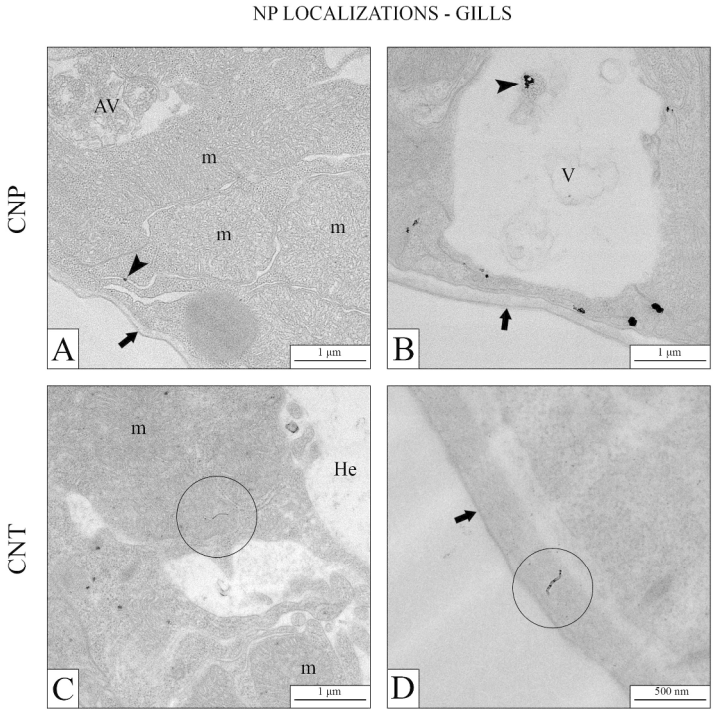

Figure 11. TEM images from CNP and CNT exposed samples showing NP localization in gills. (A) CNP aggregate between two light cells together with an autophagy vacuole. (B) A large vacuole with CNP aggregate inside and some CNP under the cuticle. (C) A CNT inside a dark cell. (D) A CNT pierced into the cuticle. AV = autophagy vacuole; m = mitochondrion; black arrowhead = NP aggregate; black arrow = cuticle; He = hemocoel.

209x297mm (300 x 300 DPI)

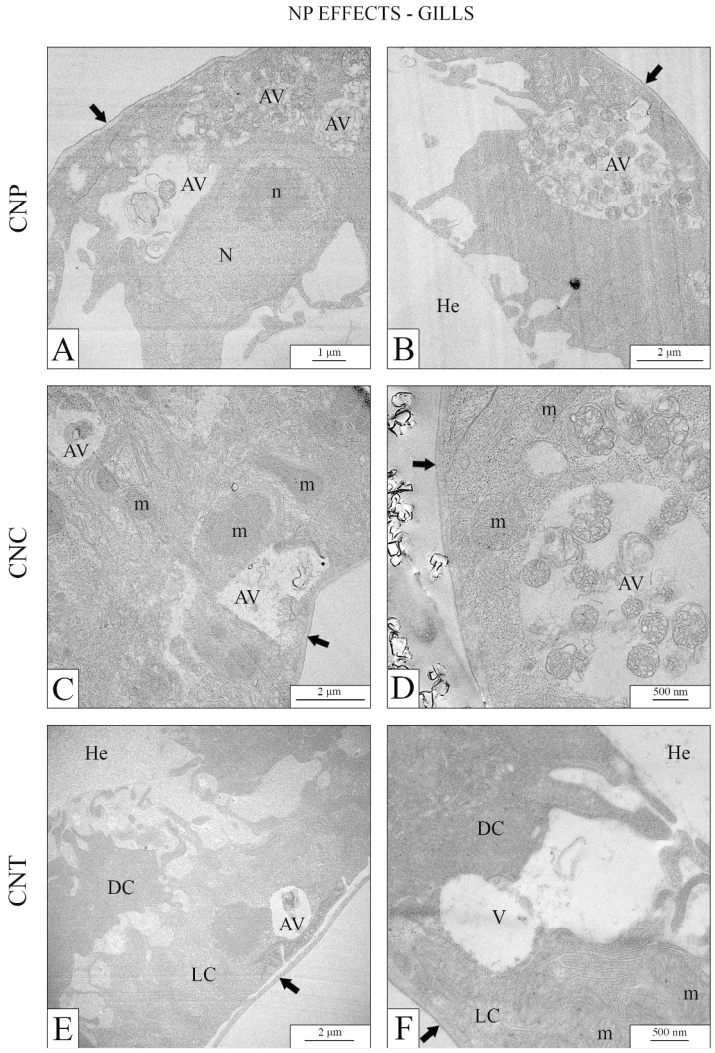

Figure 12. TEM images of gills from CNP (A-B), CNC (C-D), and CNT (E-F) exposed samples showing the effects due to NP exposure. All samples show the presence of differently sized autophagy and empty vacuoles. Black arrow = cuticle; AV = autophagy vacuole N = nucleus; n = nucleolus; He = hemocoel; m = mitochondrion; DC = dark cell; LC = light cell; V = vacuole.

209x297mm (300 x 300 DPI)

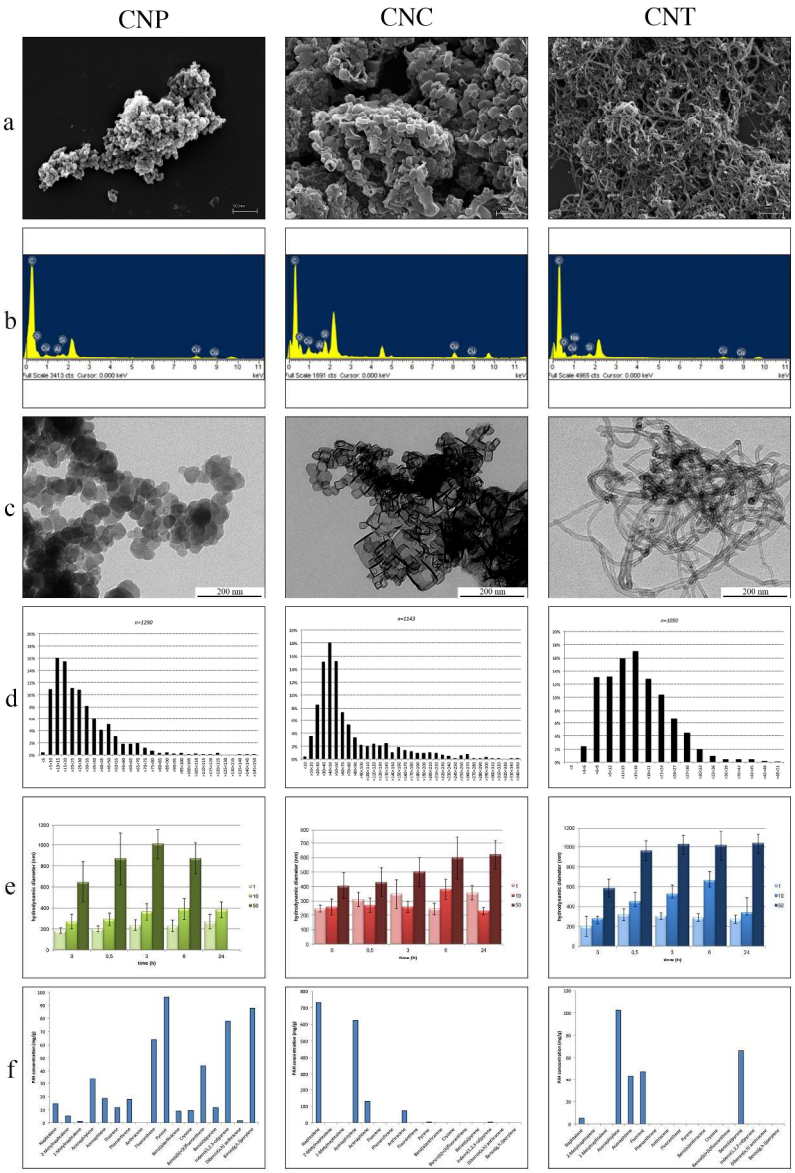

209x297mm (300 x 300 DPI)

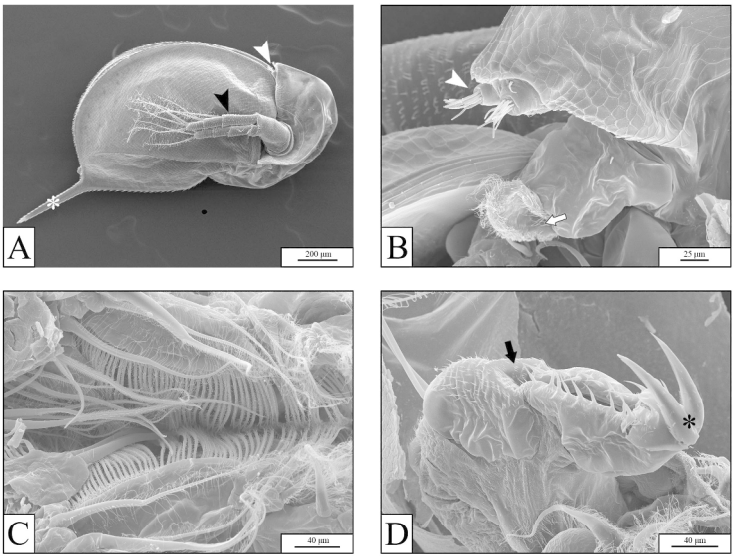

209x297mm (300 x 300 DPI)

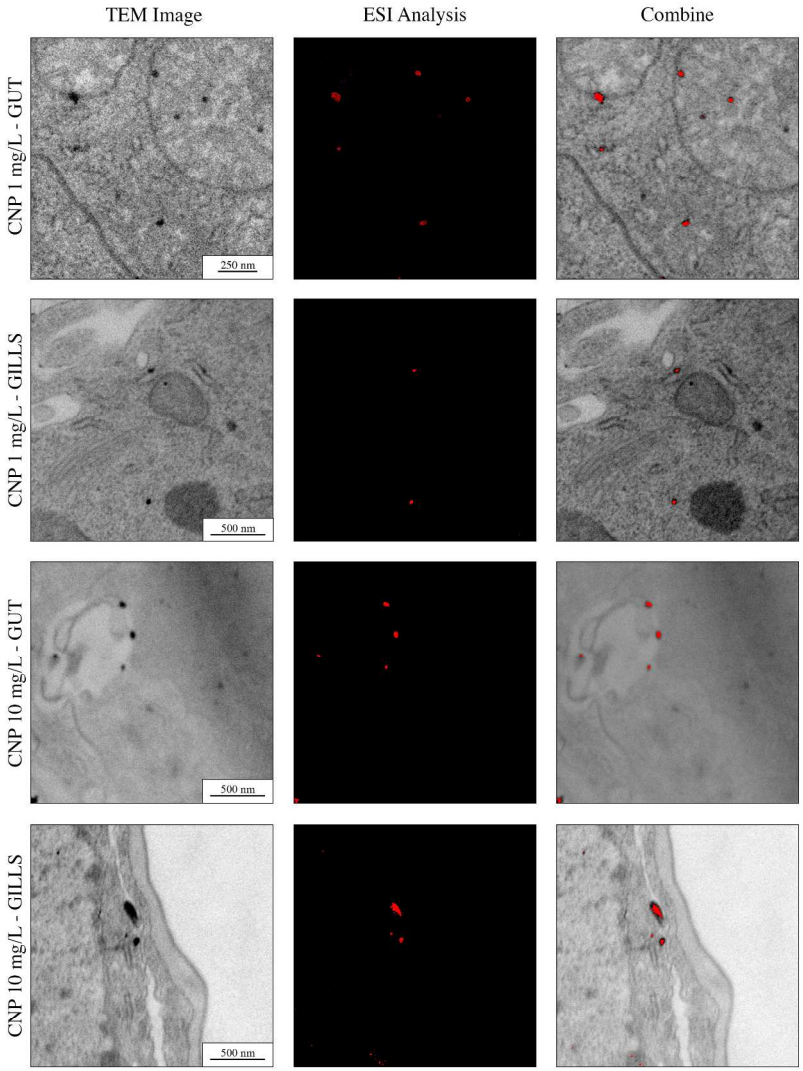

209x297mm (300 x 300 DPI)